Revision submitted to *J. Appl. Meteor. Climatol.*, Man. No. JAMC-12592, as of 22 Jan 2010

Reconstruction of near-surface tornado wind fields from forest damage

Veronika Beck[1,2,*], and Nikolai Dotzek[2,3,†]

[1] Physik-Department T34, Technische Universität München,
85748 Garching, Germany

[2] Deutsches Zentrum für Luft- und Raumfahrt (DLR), Institut für Physik der Atmosphäre,
Oberpfaffenhofen, 82234 Wessling, Germany

[3] European Severe Storms Laboratory (ESSL),
Münchner Str. 20, 82234 Wessling, Germany

Received 9 April 2009, revised 11 December 2009, in final form 22 January 2010

[*] *Present Affiliation*: Max-Planck-Institut für Biogeochemie, Hans-Knöll-Str. 10, 07745 Jena, Germany, eMail: vbeck@bgc-jena.mpg.de.
[†] *Corresponding Author*: Dr. Nikolai Dotzek, Deutsches Zentrum für Luft- und Raumfahrt (DLR), Institut für Physik der Atmosphäre, Oberpfaffenhofen, 82234 Wessling, Germany. Tel: +49-8153-28-1845, Fax: +49-8153-28-1841, eMail: nikolai.dotzek@dlr.de, http://www.essl.org/people/dotzek/

Abstract

Tornado intensity is usually inferred from the damage produced. To foster post-event tornado intensity assessments, we present a model to reconstruct near-surface wind fields from forest damage patterns. By comparing the structure of observed and simulated damage patterns, essential parameters to describe a tornado near-surface wind field are derived, such as the ratio G_{max} between circular and translational velocity, and the deflection angle α between peak wind and pressure gradient. The model consists of a wind field module following the Letzmann analytical tornado model and a tree module based on the mechanistic HWIND tree model to assess tree breakage. Using this method, the velocity components of the near-surface wind field, the track of the tornado centre and the spatial distribution of the Fujita-scale along and across the damage path can be assessed. Necessary requirements to apply the model are knowledge of the tornado translation speed (e.g., from radar observations) and a detailed analysis of the forest damage patterns. One of the key findings of our analysis is that the maximum intensity of the tornado is determinable with an uncertainty of only $(G_{max} + 1)$ times the variability of the usually well-known tornado translation speed. Further, if Letzmann's model is applied and the translation speed of the tornado is known, the detailed tree model is unnecessary and could be replaced by an average critical velocity for stem breakage v_{crit} independent of the tree species. Under this framework, the F3 and F2-ratings of the tornadoes of Milosovice, Czech Republic, on 30 May 2001, and Castellcir, Spain, on 18 October 2006, respectively, could be verified. For the Milosovice event, the uncertainty in peak intensity was only ± 6.0 m s^{-1}. Additional information about the structure of the near-surface wind field in the tornado and several secondary vortices was also gained. Our model further allows distinguishing downburst damage patterns from those of tornadoes.

Keywords: Tornado; Forest damage; Near-surface wind field; Intensity; Letzmann; Risk assessment; Downburst

1 Introduction

Post-event assessment of wind fields in tornadoes or other small-scale damaging wind phenomena like downbursts (see Doswell, 2001 for an overview) is a topic of great practical and scientific relevance. Intensity, i.e. peak wind speed and subsequently the Fujita-scale rating (F-scale, e.g., Fujita, 1981, cf. Table 1), of such events is usually inferred from site surveys or aerial photography of the damage swaths. This method is not without shortcomings (cf. Doswell and Burgess, 1998; Brooks and Doswell, 2001). First, the actual strength of damaged man-made structures or vegetation may only be known approximately. Second, by focusing only on peak intensity in F-scale ratings, the relative size of the area with that peak intensity compared to the total size of the damage swath remains obscure. And third, it might be impossible to determine peak intensity in the absence of suitable damage indicators. While damaged objects provide an estimate of the lower limit of wind speeds, inference of an upper limit of wind speeds requires objects strong enough to remain undamaged by the storm.

To address these shortcomings in part, the “Enhanced Fujita” or EF-scale was implemented in the United States of America (USA) in 2007 (cf. Potter, 2007). An enhancement of the classification of tornado *damage* (not wind speeds) was attempted by introducing a much larger set of damage indicators, including vegetation, to account for the inherent variability of structural strength among buildings or tree species during a tornado event. However, the EF-scale does not yet provide adequate solutions to the above mentioned shortcomings, as discussed, for instance, by Doswell et al. (2009). With the objective to provide a physics-based wind speed scale which can be calibrated, Dotzek (2007, 2009) proposed a generic class of scales called the “Energy“ or E-scale. These E-scales are tied to quantities like wind speed v, kinetic energy ($\propto v^2$) or power dissipation ($\propto v^3$, sometimes also referred to as “wind energy potential” or “loss potential”). Yet irrespective of the scale used to rate tornadoes and other damaging wind events, for their classification regarding peak wind speeds and spatio-temporal structure of the wind fields, methods have to be devised to reconstruct the near-surface wind fields.

The strength of such wind field reconstructions is to aid risk assessments by the insurance industry, emergency managers or forest authorities (cf. Gardiner et al., 2009; Peltola et al., 2009). With a similar approach as in our wind field model presented here, Wurman et al. (2007) superimposed representations of actual tornado wind fields on densely populated areas in the USA, like Chicago. Their risk analysis led to rather dramatic estimates of damage and fatalities and initiated a lively scientific debate (Brooks et al., 2008;

Blumenfeld, 2008; Wurman et al., 2008a,b). An approach analogous to the one for urban areas is also possible for risk analysis of potential damage to forests. Simulations of tornadoes passing over forests can be done to calculate the number of downed trees due to stem breakage or overturn. In conjunction with tornado intensity distributions (Dotzek et al., 2005), this could support the forest industry in developing adaptation concepts, for instance optimising insurance, to minimise the financial burden from forest damage by severe local storms – either occurring as individual entities or embedded in frontal bands of synoptic-scale cyclones.

While there are advanced numerical simulations of near-surface tornado dynamics over terrain without vegetation (Lewellen and Lewellen, 2007; Lewellen et al., 2008), the simulation of tornado damage in forests was recently taken up by Holland et al. (2006). They performed simulations of tornado forest damage patterns with a simple vortex model and a differentiated tree model. In their approach, they reinvented parts of much earlier, analytical work by Johannes Letzmann in the 1920s and 1930s (Dotzek et al., 2008). In Europe, tree damage had always been accounted for in tornado damage assessments (cf. Wegener, 1917). Consequently, Letzmann (1923, 1925) developed his analytical model of tornado near-surface wind fields and proposed it also as a procedure for wind field reconstruction from forest damage patterns. In the 1930s, he further devised detailed guidelines for in situ and aerial forest damage assessments which would provide the optimal input to his analytical model (Letzmann, 1939). His method to reconstruct tornado wind fields was occasionally applied in Europe to determine tornado wind field velocity components until the 1970s (Müldner, 1950; Rossmann, 1959; Euteneuer, 1970). Yet, in general, Letzmann's achievements had already started to fall into oblivion during and soon after World War II and were only rediscovered by Peterson (1992a,b), see Dotzek et al. (2000, 2008). In the USA, forest damage patterns have been documented and analyzed in a few case studies (Hall and Brewer, 1959; Budney, 1965; Forbes and Wakimoto, 1983; Fujita, 1989; Peterson, 2003). Some of these had also made brief reference to Letzmann's work, similar to Holland et al. (2006). More recently, Letzmann's work was credited by Lee and Wurman (2005), Wurman and Alexander (2005), as well as by Bech et al. (2007, 2009) who performed a simulation of the forest damage of the Castellcir tornado in Spain, which will also serve as a case study here.

The present paper summarises the work by Beck (2008) and is organised as follows: In Sec. 2, the setup and validation of the model are explained. Application and verification of the method is demonstrated in Sec. 3 via damage analysis and reconstruction of the near-surface wind fields in the tornadoes of Milosovice, Czech Republic, on 31 May 2001 and Castellcir, Spain, on 18 October 2006. Sec. 4 provides a discussion of our results, also addressing the distinction between tornado and downburst damage patterns. Sec. 5 presents our conclusions.

2 Model description and validation

2.1 Letzmann's analytical wind field model

Letzmann (1923) developed a complete analytical three-dimensional tornado model with a linear velocity increase in the tornado core (i.e., solid body rotation) and hyperbolical velocity decay in the tornado mantle for the tangential (v_θ) and radial (v_r) velocity components of the tornado wind field (Fig. 1, cf. Beck et al., 2008). The vertical velocity component can either be constant or variable for barotropic or baroclinic vortices, respectively. For the determination of the tree damage patterns, Letzmann (1923) used a projection of the three-dimensional tornado wind field onto the horizontal x,y-plane. In the resulting model, v_θ and v_r are described by the following relations (Letzmann, 1923):

$$v_{r,\theta} = v_{r,\theta\max}\left(\frac{r}{R_{\max}}\right)^{\gamma} \quad , \qquad r \le R_{max} \quad , \tag{1a}$$

$$v_{r,\theta} = v_{r,\theta\max}\left(\frac{R_{\max}}{r}\right)^{\gamma} \quad , \qquad r > R_{max} \quad , \tag{1b}$$

with R_{max} indicating the radius of maximum winds, demarcating the tornado core, and $v_{r,\theta\max}$ the maximum absolute value of v_r and v_θ at $r = R_{max}$, respectively. Letzmann (1923) used the exponent γ in Eqs. (1a,b) to specify the strength of the velocity increase in the tornado core and of the hyperbolical velocity decay in the tornado mantle. For $\gamma = 1.0$ as often applied by Letzmann (1923), Eqs. (1a,b) show exactly the velocity distribution of a Rankine vortex with a linear velocity increase in the tornado core and a hyperbolical velocity decay in the tornado mantle valid for conservation of angular momentum. By measuring tornado radial velocity profiles with the help of mobile Doppler radars, an exponent of $\gamma \approx 0.6$ was detected recently, suggesting that angular momentum might not be conserved in real tornadoes (e.g., Bluestein, 2007). While $\gamma = 0.6$ has been used as well, most results presented here assume $\gamma = 1.0$. Additionally, there is the translation velocity v_{trans} of the tornado which was assumed constant for simplicity by Letzmann (1923) and in the present work.

Contrary to other mathematical descriptions of the Rankine vortex (e.g., Kanak, 2005), v_r and v_θ of the Letzmann (1923) model are determined by three parameters: v_{trans}, G_{max} and α. Here, G_{max} indicates the ratio between circular (v_{cir}) and translation velocity (v_{trans}) components of the tornado wind field. The circular velocity component is defined as the superposition of v_r and v_θ. Its further superposition with v_{trans} leads to the total velocity v of the tornado wind field. Furthermore, α denotes the angle between the direction of the wind (v) and the pressure gradient $\nabla p \propto v_r$ at the point of maximum velocity, where v_r and v_{trans} are perpendicular, as illustrated in Fig. 1.

The dependence of the wind field on the parameters G_{max} and α is shown in Fig. 2. By varying the parameter G_{max}, genesis of two calm points (Letzmann, 1923) of zero total velocity, one central and one marginal point, occurs at a value of $G_{max} = 1$ (Fig. 2b). For higher values of G_{max}, the distance between the two calm points increases monotonically (Fig. 2c). For the variation of the angle α, a change from inflow towards the vortex centre (Fig. 2d) in early stages of the tornado lifecycle to outflow from the vortex centre (Fig. 2f) during the decaying stage is notable at a value of $|\alpha| = 90°$ (Fig. 2e).

Tree damage patterns that depend on the parameters G_{max} and α have been derived by Letzmann (1923) by using the method of "individual circles" (cf. Peterson, 1992a). Letzmann calculated the theoretical fall direction of the trees with respect to the direction of the translation velocity of the tornado (Fig. 3a). To characterise the tree damage patterns, a tree fall angle ψ describing the deflection of downed trees from the direction of tornado translation (cf. Fig. 1) was derived by Letzmann (1923), with φ indicating the angle between v_{cir} and v_{trans}:

$$\cos\psi = \frac{v_{trans} + v_{cir}\cos\varphi}{\sqrt{v_{trans}^2 + v_{cir}^2 + 2v_{trans}v_{cir}\cos\varphi}} \quad . \tag{2}$$

A divergence line in the vortex is always characterised by one or more downed trees with $\psi = 0°$ along a cross-section perpendicular to the direction of translation. On the contrary, a convergence line is indicated by such fallen trees with either $\psi = 0°$ or $\psi = 180°$ (Letzmann, 1923). Fig. 3a demonstrates the tree damage patterns for $G_{max} = 2.0$ and varying angles α for different critical velocities for stem breakage v_{crit}. For the determination of v_{crit}, the tree model described in Sec. 2.2 is used.

For low v_{crit} (< 20.0 m s^{-1}, upper treefall pattern rows) in Fig. 3, a tree with $\psi = 180°$ occurs for all angles $0° < |\alpha| < 90°$, while for higher v_{crit} (middle and lower treefall pattern rows for each angle α) it is replaced by a tree with a falling angle $\psi = 0°$. The location of this tree in Fig. 3 with $\psi = 180°$ and $\psi = 0°$, respectively, moves to the left side of the damage pattern for low v_{crit} and to the right side for high v_{crit} (> 70.0 m s^{-1}) with increasing absolute values of α. Both cases lead to a convergent tree damage pattern. This convergent tree damage pattern is consistent with the inflow structure of the near-surface tornado wind field for angles $|\alpha| < 90°$ (cf. Fig. 2d).

At $|\alpha| = 90°$ trees close to $\psi = 0°$ occur on the right side of the damage pattern in Fig. 3. They indicate a divergence line and result from the dominating tangential flow of the tornado wind field. For $|\alpha| > 90°$, the locations of these trees move to the centre of the damage pattern. The related wind field in Fig. 2f has a divergent structure demonstrating the outflow from the tornado vortex core. However, the separation into two calm points for $G_{max} \geq 1$ in Figs. 2c-f is not reflected in the tree damage patterns of Fig. 3 (cf. Letzmann, 1923) due to the low wind speeds in these regions.

The tree damage patterns as a function of the parameters G_{max} and α have been classified by different swath types (Letzmann, 1923, 1925). Fig. 4 illustrates these tree damage patterns and corresponding streamline patterns for the different swath types. For $|\alpha| > 90°$, all swath types show a divergent damage pattern while for $|\alpha| < 90°$, the convergent damage patterns of the individual swath types differ, depending on G_{max} and v_{crit}. For values of $G_{max} < 1$, swath type I has a weak convergent damage pattern and is independent of the value of v_{crit}. For high values of $G_{max} > 3.5$, swath type IV is clearly identified by a tree with a fall angle $\psi = 180°$ in the tree damage pattern independent of v_{crit}. Swath type II and swath type III occur for values of G_{max} between 1.0 and 3.5. Tree damage patterns classified as swath type II have small or moderate values of v_{crit}, i.e., $v_{crit} < 70.0$ m s^{-1}, and are indicated by locations of a tree with $\psi = 0°$ moving to the left side of the damage pattern for increasing $|\alpha|$. Swath type III is found for values of $v_{crit} > 70.0$ m s^{-1} indicated by locations of the tree with fall angle $\psi = 0°$ shifting to the right side of the damage pattern for increasing $|\alpha|$.

2.2 Tree damage model

Based on various tree parameters (for actual values see Sec. 2.3), like tree height h_t, tree diameter at breast height d_{BH}, and modulus of rupture M_{rup}, the bending moment B_{max} and the tree resistance for stem breakage M_{crit} are calculated and compared. From this comparison, the critical velocity for stem breakage v_{crit} is evaluated. This algorithm is based on the HWIND model of Peltola and Kellomäki (1993). First, the forces contributing to B_{max} have to be considered. The tree is divided into Δz = 1 m segments in the vertical. The areas of the stem and the crown are approximated by a rectangle and two isosceles triangles, respectively (Fig. 5). To calculate the drag force F_W on the tree, a modified logarithmic wind profile (Prandtl, 1925) within and above the forest was used to derive the horizontal velocity v_h for each tree segment:

$$\bar{v}_h = \frac{v_*}{\kappa} \ln \frac{z}{z_0} \ln \frac{h_t}{z_0} \quad . \tag{3}$$

In Eq. (3), v_* indicates the friction velocity, z the height above ground (and also the number of the tree segment), h_t denotes the tree height, z_0 is the roughness length, and κ = 0.4 is the von Kármán constant. The drag force for each 1-m segment is (Peltola and Kellomäki, 1993):

$$F_w(z) = \frac{1}{2} c_d \rho \bar{v}_h^2 A(z) \quad . \tag{4}$$

Here, c_d indicates the drag coefficient, ρ is the air density and A denotes the windward-projected cross section of each 1-m segment. If the velocity is high enough, the tree (i.e., foliage and smaller branches) will become streamlined and the effective cross sectional area of the crown is reduced. For wind speeds less than 11.0 m s^{-1}, A is reduced by 20%, while for wind speeds greater than 20.0 m s^{-1} the reduction increases to 60%. In between, Peltola and Kellomäki (1993) used a streamlining factor S_t to describe the reduction:

$$S_t(z) = \frac{10.0}{\bar{v}(z)} - 0.10 \quad . \tag{5}$$

If the tree not only becomes streamlined but also starts to bend over for higher wind speeds, the gravitational acceleration g leads to a force F_G on the overhanging crown:

$$F_G(z) = m_c \, g \quad . \tag{6}$$

The crown green mass m_c and the stem mass m_s follow from Baldwin (1987). The tree deflection x and the maximum bending moment B_{max} per segment are again based on Peltola and Kellomäki (1993):

$$B_{\max}(z) = f_{gust} f_{gap} \left[F_W(z) \Delta z + F_G(z)\, x(z) \right] \quad . \tag{7}$$

The gust-factor f_{gust} indicates the ratio between the maximum and the mean bending moment and was determined from wind tunnel experiments (Gardiner et al., 1997), while the gap-factor f_{gap} characterizes the effects of variable upwind gaps in the tree stand (Holland et al., 2006). The total bending moment for each tree is the sum of all bending moments per tree segment, and is compared to the resistance of the tree M_{crit} (Peltola and Kellomäki, 1993) to determine v_{crit}:

$$M_{crit} = \frac{\pi}{32} M_{rup} d_{BH}^3 \quad . \tag{8}$$

2.3 Model implementation

The model for the simulation of tree damage patterns consists of a wind field module and a tree damage module. The structure of the model and the module interrelations are outlined in Fig. 6. In the typical setup, the calculations are done for a 400 m x 400 m horizontal domain with a grid spacing of $\Delta x = \Delta y = 10$ m. For the tree module, the domain is extended to three dimensions with a height of 30 m and a grid size of $\Delta z = 1$ m in the vertical direction.

In the first part of the model, the tree module, v_{crit} is derived. The bending moment and the tree resistance are calculated from an iterative process, using several tree parameters and an initial guess for the wind speed. If the bending moment exceeds the tree resistance, the iteration ends, otherwise the velocity is incremented by 0.5 m s^{-1} steps. According to the HWIND model (Peltola and Kellomäki, 1993) the tree resistance for stem breakage can be replaced by the tree resistance for overturn to calculate the critical velocity for tree overturn $v_{crit,o}$. If tornado damage patterns with only uprooted trees occur, the appropriate tree resistance for tree overturn is used for the simulation of tree damage patterns (Beck, 2008).

Values of v_{crit} calculated individually for each tree are then used by the wind field module to simulate the tree damage patterns. The wind field module produces an instantaneous velocity at each grid point which is compared to v_{crit}. If the instantaneous velocity of the wind field exceeds v_{crit}, the tree is considered to be downed and the fall direction is assumed to be the instantaneous direction of the wind field at the corresponding point, in accordance with Letzmann (1923), Holland et al. (2006) and Bech et al. (2009).

The vortex representing the tornado wind field starts at the southern domain boundary and then moves across the domain in positive *y*-direction with translation speed v_{trans}. To avoid undersampling, the time step Δt was limited to:

$$\Delta t \leq \frac{\Delta y}{v_{trans}} \quad . \tag{9}$$

Initial conditions for the tree and the wind field module have to be specified as well. For the tree module, either a random or a homogeneous distribution of tree age has been provided. Furthermore, various tree parameters depending on the tree species have to be set, for instance for Norway spruce (*picea abies*): tree height h_t = 24.6 m, tree age a = 70 yr, diameter at breast height d_{BH} = 0.30 m, modulus of rupture M_{rup} = 39.1 MPa, modulus of elasticity E = 7000 MPa, gap size g_s= 15 h_t (accounting for the upwind gap or fetch on the forest edge in the calculation of the gap factor f_{gap}), and drag coefficient c_d = 0.29. For the calculation of the gust factor f_{gust}, the distance between two trees is set to 2.5 m, so every fourth tree is resolved by the model grid.

For the wind field module, both G_{max} and α depend on the simulated velocity field. The radius of the tornado core is set to R_{max} = 75 m, and v_{max} = 80.0 m s^{-1} is the maximum velocity of the tornado (including v_{trans}). Finally, the coordinates of the starting point of the vortex centre are set to (x_c, y_c) = (0, -200) m.

2.4 Model validation

The theoretical tree damage patterns of Letzmann (1923) are compared to the tree damage patterns produced by the model in Fig. 3 for G_{max} = 2.0 and different angles α. Letzmann (1923) derived tree damage patterns for each angle α for four different tree resistances, varying v_{crit} as multiples of the translation velocity of the tornado (Fig. 3a). Our reproduced tree damage patterns in Fig. 3b (cf. Beck, 2008) have been simulated for three different magnitudes of v_{crit} calculated from the tree module. Fig. 3b shows the location of a tree with fall angle ψ = 180° for $|\alpha|$ < 90° moving to the left side of the tree damage pattern for small v_{crit} in the same way as depicted in Fig. 3a. For high v_{crit}, in both panels of Fig. 3, the width of the damage path is reduced and the tree location with ψ = 0° moves to the left for $|\alpha|$ < 90°. Crossed trees at $|\alpha|$ = 60° occur in both panels as well. For $|\alpha|$ > 90°, a divergent damage pattern with a tree location having fall angle ψ = 0° that moves to the left flank of the track is also notable for both the Letzmann (1923) graph and our simulation.

The absolute values of v_{crit} for both tree damage patterns do not correspond exactly, as our absolute value of v_{crit} for moderate and high intensities in Fig. 3b is presumably smaller compared to Letzmann's values in Fig. 3a. Yet, in summary, we argue that the structure of the damage patterns from Letzmann (1923) and Beck (2008) are very similar in case of equal values for v_{crit}. Now the developed model can be applied to determine tornado intensities from forest damage and comparison to other models, like those of Holland et al. (2006) or Bech et al. (2009).

3 Forest damage analyses

To reconstruct tornado near-surface wind fields and to determine tornado intensities from forest damage patterns, the observed tree damage patterns of two tornadoes are analysed here with respect to their relevant parameters. Further applications of our model were presented by Beck (2008). Note that in order to use this method for wind field reconstruction of tornadoes, it is essential to either rely on aerial photographs (cf. Dotzek et al., 2007; Dotzek and Friedrich, 2009) of the forest damage patterns or Letzmann's "method of lines" in ground surveys, as already emphasised by Letzmann (1939). Otherwise, the inherent parallax errors will make it rather difficult to determine the location of the fallen trees with the necessary precision. If this condition is satisfied (as in our two cases below) then the general procedure to apply our model to an actual forest damage observation is as follows.

First, an estimation of the angle α is done by inspecting if the damage patterns are convergent ($|\alpha| < 90°$) or divergent ($|\alpha| > 90°$). From this estimation, the stage of the tornado life cycle (Letzmann, 1923; Davies-Jones, 1986) can readily be identified. The sense of vortex rotation (cyclonic or anticyclonic) is derived from comparison of the damage patterns to the cyclonic swath types of Letzmann (1923, cf. Fig. 4). From radar or ground observations, the translation direction is inferred and v_{trans} is calculated, using storm propagation as a proxy for tornado translation. In the next step, downed trees with $\psi = 0°$ and $\psi = 180°$ with respect to the direction of translation have to be identified in the observed forest damage patterns. From the number of convergence or divergence lines reflected in the pattern of broken trees, the values G_{max} and α can be quantified. The radius R_{max} of the tornado core is estimated from the width of the damage path in consecutive trial simulations. The observed damage patterns using the tree parameters from Sec. 2.3 have to be simulated iteratively by varying the initial estimates of G_{max}, α, and R_{max}. From this, the structure and intensity of the tornado wind field is recalculated until the qualitative agreement between the simulated tree fall pattern and the observed damage swath is maximised.

3.1 Milosovice tornado, 31 May 2001

An F3 tornado occurred near Milosovice–Velka Paseka in the Czech Republic on 31 May 2001 with a path width of 400-500 m and path length of 16 km (www.essl.org/ESWD/, cf. Dotzek et al, 2009). Besides the main vortex, three smaller vortices were observed (www.chmi.cz/torn/cases/20010531/20010531.html and Martin Setvák, 2008, pers. comm.). The translation velocity of the thunderstorm cell producing the tornado was estimated from Czech Hydrometeorological Institute (CHMI) radar observations (not shown) to 16.5 ±1.0 m s^{-1}. This is also assumed as v_{trans} of the tornado[1]. The radar observations confirmed that the thunderstorm propagated to the east-south-east, in line with the main tornado damage swath. The aerial photo of the forest damage (Fig. 7a) shows the division of the forest damage patterns according to the four vortices. The main vortex (1) is identified with the tornado, while the damage patterns of the other three vortices (2)–(4) surround the damage pattern of the main vortex.

The comparison between the simulated and the observed damage patterns of the main tornado is illustrated in Fig. 8 as well as the distribution of the F-scale along the damage path for these simulations. By comparing the observed damage patterns of the main tornado with the swath types of Fig. 4, a divergent damage pattern has been found. This evidence supports $90° < |\alpha| < 180°$. By variation of the other parameters G_{max} and R_{max}, the observed damage pattern is approached in consecutive simulations. For the simulations, the tree parameters for Norway spruce as mentioned in Sec. 2.3 have been used. Comparing the three damage patterns of the main vortex, Fig. 8a shows a more divergent damage pattern than Fig. 8b and Fig. 8c. The width of the damage path is constant throughout the damage pattern leading to a constant R_{max} of the vortex core. The best correlation to the observed damage pattern can be found for G_{max} = 4.0-5.0, $|\alpha|$ = 140°-150°, and R_{max} = 80 m. Reasons for the not completely exact match of the observed and simulated damage patterns might be that the model does not take into account any interaction of falling trees. Further, terrain effects that might lead to a higher damage level downhill or a lower damage level uphill due to frictional and gravitational forces are also not included in the model. Therefore, not all variation in the structure of the damage patterns can be reproduced by the model. In the Milosovice tornado, parts of the broken trees were also observed on a downsloping terrain which probably caused stronger damage and slightly different treefall patterns compared to our simulation.

For vortex 2, an anticyclonic rotation and a strongly divergent damage pattern are notable. Vortex 3 is found to have smaller spatial extension and cyclonic sense of rotation similar to the main vortex. Further, a central convergence line and a fast-changing structure of the damage patterns have been detected. Vortex 4 shows anticyclonic rotation with a strongly divergent damage pattern. A detailed overview over the parameters used for the simulations of the damage patterns of the different vortices are given in Table 2.

From the simulation of the damage patterns, the vortex trace (centreline of damage swath) and its divergence and convergence lines can be located. Thus, we now focus on the location of the trace as well as these divergence and convergence lines as illustrated in Fig. 7b for all four vortices. In vortices 1, 2 and 4, the divergence line is indicated by a tree with $\psi = 0°$ while for vortex 3, the tree with $\psi = 0°$ indicates a convergence line. Considering vortex 1 and 4, the divergence line is located on the right and left side of the trace of the tornado, respectively. For vortices 2 and 3, the divergence and convergence lines, respectively, coincide with the trace of the vortex.

From the simulation, the maximum velocity of the main vortex is derived by using the translation velocity component v_{trans} of the main vortex determined by radar observations and the relation between v_{cir}, v_{trans} and G_{max} (Letzmann, 1923):

$$G_{max} = \frac{v_{cir}}{v_{trans}} \quad . \tag{10}$$

For the three smaller vortices around the main vortex, the individual translation velocity components are unknown. Nevertheless, a lower limit of the maximum velocity can be calculated based on v_{crit} from the tree module for these vortices. A summary of all calculated velocity components is given in Table 2.

Fig. 9 illustrates the reconstructed near-surface wind fields corresponding to the four vortices. The wind fields of the main vortex (Ia-Ic) illustrate the largest spatial extension of all vortices. Its structure does not change significantly. An anticyclonic rotation in the wind fields of vortex 2 (IIa-IIc) is shown. The reconstructed wind fields of vortex 3 show parts of the evolution of a tornado life cycle: the pattern changes from a convergent inflow in the organising and formation stage of a tornado to a pure tangential flow in the mature stage of a

[1] In the error calculation in Sec. 4, we also consider the effects of a discrepancy between the tornado propagation

tornado (cf. Hall and Brewer, 1959). The wind fields of vortex 4 (IVa,b) are similar to those of the main vortex, but with smaller spatial extension and anticyclonic rotation.

From the reconstructed near-surface wind fields, an F-scale distribution within the domain can be derived. Fig. 8 shows the resulting distribution for the main vortex indicating a widespread F3 zone (71-93 m s^{-1}) and even an F4 zone (93-117 m s^{-1}) for one of the damage patterns of the main vortex with the most widespread and extensive damage. Two of three damage patterns yield a peak intensity of F3, and damage of F4 intensity is limited to only a few points. The classification of the main vortex as a tornado is verified by obtaining a characteristic divergent damage pattern at the end stage of a tornado life cycle and a path width consistent with high-F3 tornadoes (Brooks, 2004). Thus, in total, our model verifies the classification of the tornado as an F3 tornado.

3.2 Castellcir tornado, 18 October 2006

The F2 Castellcir tornado (Aran et al., 2009; Bech et al., 2009) occurred in Catalonia, Spain, on 18 October 2006 with a damage path length of about 4 km from south-west to north-east and a maximum damage path width of 260 m. After the tornado, a microburst occurred further to the north-east. In this case, a damage analysis was performed along the total damage path, allowing for a more detailed determination of tornado intensity compared to the analysis of only a single prominent part of the damage path, like for the Milosovice tornado. The translation velocity component v_{trans} of the Castellcir thunderstorm cell was derived from radar observations as 11.1 m s^{-1}, see the detailed analysis of the tornado and its damage by Bech et al. (2009). In particular, it is fortunate that Bech et al. (2009) used a Letzmann-type model similar to ours, so comparing our analysis of the Castellcir tornado to their results will serve as additional verification of our model and help to substantiate the intensity assessment for this case.

The left column of panels in Fig. 10 illustrates the reported locations of the downed trees along the tornado damage path in five selected regions. This can be compared to Bech et al. (2009, their Fig. 8) showing the full damage swath and grouping it slightly differently in eight subregions. Their region 1 (F0 intensity) corresponds to our region I), while their regions 3 and 4 (F1 and F2 intensity) relate to our regions II) and III), and finally, their regions 6 and 7 (F1 intensity) roughly correspond to our regions IV) and V). Bech et al.

---

and the translation of the thunderstorm cell.

(2009) did not derive G_{max} and α in all regions of the damage path, but they reported G_{max} = 2.0, α = 0° in region 1, and G_{max} = 4.0, α = -90° in region 4.

Our modelling results for the tree damage patterns (central column of Fig. 10) corroborate and extend these results. A summary of all derived velocity components is shown in Table 3 while the tree parameters used for the simulations are the same as in Sec. 2.3. The results show for region I) a convergent damage pattern (α = 0°) typical for the beginning of a tornado life cycle, while regions II) to V) are dominated by mainly tangential flow ($|\alpha|$ equal or close to 90°). Also our derived values for G_{max} are well in line with Bech et al. (2009). Yet, we were able to obtain the vortex parameters in a larger number of path regions. From the derived parameters, the F-scale distribution along the path (right column of Fig. 10) provides evidence for first F0 and then mostly F1 intensity with a very small embedded F2 zone in regions II) and III). This is exactly in line with Bech et al. (2009). Therefore, the F2 rating of the tornado is verified even if the F2 zone is very small (Beck, 2008).

In addition, the cyclonic sense of rotation of the tornado was also confirmed, and R_{max} = 50 m in this case is smaller compared to R_{max} of the Milosovice tornado. Note that terrain effects not included in the model might have played an important role for the specific local structure of the damage patterns, as the terrain elevation along the tornado track varied by about 200 m (Bech et al., 2009).

4 Discussion

The model developed here allows for a more accurate determination of the tornado intensity compared to the classification of tornado intensity based on pure damage analysis (Fujita, 1981). Additionally, detailed information about the type of the tornado near-surface wind field and the location of the tornado trace are gained. From the simulation and comparison of the tree damage patterns to the observed damage patterns, the tornado parameters G_{max}, α and R_{max} are derived. Together with the translation velocity of the tornado as evaluated from radar or ground observations, the maximum intensity of the tornado can be calculated. In our cases, the thunderstorm translation speed was determinable with an uncertainty of ±1.0 m s^{-1}. This also takes into account small deviations of the tornado propagation from the translation of parent thunderstorm cell, for instance, by weak meandering of the tornado. The error in the estimation of the maximum tornado velocity can readily be tied to the uncertainty of the translation velocity (Beck, 2008):

$$\Delta v_{max} = (G_{max} + 1)\ \Delta v_{trans} \quad . \qquad (11)$$

As G_{max} does not appear to exceed values of $G_{max} \approx 6.0$ (already suggested by Letzmann, 1923, 1925, and consistent with our cases peaking at $G_{max} = 5.0$), the highest intensity of the Milosovice tornado is determinable with a maximum error of $\Delta v_{max} \approx \pm 6.0\ \mathrm{m\ s^{-1}}$. This accuracy is less than one half-step of the F-scale (Table 1). With prior knowledge of the translation velocity and the subsequent derivation of the relevant tornado parameters using our model, the near-surface wind field of the tornado can be completely reconstructed, and conclusions on the life cycle stage of the tornado from confluent early stages to the more diffluent decay can be drawn.

Provided the translation speed is known, the biggest advantage of the Letzmann-type model for tornado cases is its independence of the tree species and other tree parameters (Beck and Dotzek, 2009). For tornado vortices, the structure of the damage patterns itself already allows the reconstruction of all relevant wind field parameters, provided that a sufficient amount of trees was downed. So in this case, the detailed tree model is unnecessary, and the inherently high uncertainties of tree models with respect to wood parameters, tree species, age distribution, or even soil type and moisture can be excluded. The only necessary parameter for simulating tree damage patterns is an average value for the critical velocity for stem breakage v_{crit}. In our case, it was derived from the tree model. An evaluation of the uncertainties in v_{crit} from the tree module based on the HWIND model was given by Beck (2008): To adapt the HWIND model to more realistic conditions, a Gaussian distribution of the modulus of rupture M_{rup} was introduced. This led to an uncertainty of $\Delta v_{crit} = 20.0$-$31.0\ \mathrm{m\ s^{-1}}$ for a 90% confidence level of M_{rup}, as deemed necessary to describe the conditions in tree stands realistically.

Of course, such uncertainties larger than one full step of the F-scale lead to a less reliable determination of tornado intensities. Instead, the independence of tree parameters in tornado cases gives our model its accuracy. Note also that our model is not limited to the simulation of forest damage patterns for tornado intensity determination. It can likewise be used to simulate crop damage patterns to determine the tornado intensity, as already argued by Letzmann (1923).

Compared to the simulated tornadic forest damage patterns of Holland et al. (2006), our model shows some notable differences. In both cases, the tree module is based on the HWIND model of Peltola and Kellomäki (1993). However, contrary to the random age distribution of trees used by Holland et al. (2006), both random and homogeneous age distributions of either loblolly pine (*pinus taeda*) or Norway spruce (*picea abies*) are used, as homogeneous age distributions better fit the conditions of many forests in Europe (Letzmann, 1923; Hubrig, 2004, 2008, pers. comm.).

Holland et al. (2006) referred to Letzmann (1923), but used v_r, v_θ, and v_{max} to describe a Rankine vortex for their simulation of forest damage patterns. In our model, we used the full analytical tornado model and resulting theoretical tree damage patterns by Letzmann (1923) which rely on G_{max}, α and v_{max} to describe the Rankine-type vortex. Fig. 11 shows that the structure of the damage patterns of Holland et al. (2006) and our simulated tree damage patterns are similar. Yet, because of the dependence of their tornado wind field on the parameters v_r, v_θ and v_{max}, only values of $51° \leq |\alpha| \leq 90°$ have been considered by Holland et al. (2006). With our present model, the structure of divergent tornado damage patterns occurring for $90° < |\alpha| < 180°$ can also be simulated.

Comparing Fig. 11 to the theoretical damage patterns of Fig. 3a, we found that the simulated damage patterns of Holland et al. (2006) correspond to a high value of v_{crit} while our simulated damage patterns correspond to a moderate value of v_{crit}. This is confirmed by the number of convergence lines in the simulated damage patterns. The damage patterns of Holland et al. (2006) show only one convergence line with a tree of $\psi = 0°$ while our damage patterns show two convergence lines, one with a tree of $\psi = 0°$ and another with a tree of $\psi = 180°$. The damage patterns of Holland et al. (2006) contain a smaller number of broken trees. This might be due to the fact that either their value of v_{crit} for the random-age forest was higher, or that their simulation time steps exceeded Eq. (9), leading to undersampling and a non-continuous interaction between the near-surface tornado wind field and the tree stand.

Bech et al. (2009) have already used a Letzmann-type Rankine vortex depending on G_{max}, α and v_{max} for their simulation of the tornado wind fields in the Castellcir tornado. In contrast to our procedure, they determined their values of G_{max} and α from comparison of the observed tree damage patterns with the simulations of the tornado wind field. With our simulations of the Castellcir tree damage patterns, we can verify the values for G_{max} and α as evaluated by Bech et al. (2009) and also obtain values of G_{max}, and α for zones not classified by these authors: $G_{max} = 3.5$ and $\alpha = -90°$ (zone IV) and $\alpha = -70°$ (zone V), respectively.

An additional comparison by Beck (2008) of the tree damage patterns resulting from an idealised downburst simulation to that of tornadoes revealed that it is possible to obtain damage patterns of almost identical appearance. But some distinguishing features between tornado and downburst damage in forests could be identified using our model. The damage patterns of the downburst consistently show a divergent structure, while the damage pattern of the tornado usually changes from a convergent structure in the formation stage to a more divergent structure in the following stages (Letzmann, 1923). The fall angle $|\psi|$ of a divergent tornado damage pattern does not exceed 45°, while this was the case for the downburst, because here, the wind field is more divergent and the translation velocity is smaller. A third, but weaker characteristic is the spatial extension of the swath, that is, its length-to-width aspect ratio, which is generally larger for a tornado than for a downburst (e.g., Knupp, 2000). The Milosovice tornado could be verified as a tornado event, because of small fall angles in the divergent structure of the damage pattern and a path aspect ratio typical of tornadoes (cf. Brooks, 2004). Thus, simulation of the tree damage patterns also helps to discriminate between tornado and downburst events.

There are further applications of the concepts presented here, for instance, Letzmann's analytical model can also be applied to analyse the wind field structure of tropical and extratropical cyclones (Letzmann, 1925). In addition, Letzmann (1923, 1925) had already analytically examined tornado vortices with two velocity maxima in v_r and v_θ. In Fig. 12, the velocity field and the streamline patterns of a wind field with double velocity maxima are illustrated. Note that the streamlines in Fig. 12b2 show a surprising similarity to the shape of a certain class of hook echoes in radar observations of severe thunderstorms. Hook echoes are often found at low- or mid-levels in mesocyclonic storms and in particular in combination with the occurrence of a tornado (e.g., Wurman, 2002; Bluestein, 2007).

In some cases, observed hook echoes at, say, 1 to 3 km AGL display a sharp bend or "kink" (e.g., French et al., 2008, their Fig. 6g). As Letzmann's vortex model is not limited to winds near the surface, we may apply his concepts also to parts of the vortex higher up. Accordingly, the velocity fields in Fig. 12 suggest that these "kinky hooks" might result from the interaction between the tornado vortex and the mesocyclone. If so, the interior velocity maximum would belong to the tornado (misocyclone), while the exterior velocity peak would be produced by the larger mesocyclone aloft. A detailed analysis of this effect using the model presented here is the subject of ongoing work.

5 Conclusions

The method presented here allows reconstruction of near-surface tornado wind fields from the analysis of actual forest damage patterns. By simulating the observed tree damage patterns, the intensity and relevant parameters characterising the wind field can be obtained:

- The analytical tornado model of Letzmann (1923) depending on the parameters G_{max}, α and v_{trans} is perfectly suited to determine these parameters based on the forest damage patterns;
- If the tornado translation speed is known, the damage pattern completely determines the wind field and its intensity in the Letzmann model, that is, intensity can be inferred without knowledge of the actual tree stand parameters;
- The translation speed of the tornado-producing thunderstorm as determined, e.g., from radar observations may be used as a valid proxy to the tornado translation speed;
- By consecutive simulations with varying parameters G_{max}, α and R_{max} to fit the observed damage patterns, the near-surface tornado wind fields and the location of the centreline of the tornado track can be determined;
- The convergence and divergence lines first mentioned by Letzmann (1923) could be verified in the observed tree damage patterns, leading to a better damage classification;
- Analyses of the observed tree damage patterns of the Milosovice and Castellcir tornadoes led to a verification of their F3- and F2-ratings, respectively;
- The distribution of the F-scale along and across the path reveals the areal percentage of maximum intensity and may be used in risk models;
- Compared to the determination of tornado intensities from damage, the maximum velocity of the Milosovice tornado was determinable with an uncertainty of only ± 6.0 m s^{-1}, less than a half-level of the F-scale, while in general, the relation $\Delta v_{max} = (G_{max} + 1)\ \Delta v_{trans}$ holds. This is encouraging, given the fact that the main objective of the method was to reconstruct the tornado near-surface wind field structure.

Aside from the ongoing work applying our model to vortex levels aloft with a double wind maximum to explain the often-observed “kinky hooks”, a fruitful option for future work would be to extend the Letzmann formalism to three dimensions as already outlined by Letzmann (1923) and to dynamically simulate the lowest, say, 100 m of an advancing tornado.

Acknowledgements

The authors are grateful to Martin Setvák, Czech Hydrometeorological Institute, for providing radar images and aerial photographs of the Milosovice tornado, and to Joan Bech, Meteorological Service of Catalonia, for information on his Castellcir tornado analysis. Leigh Orf, Central Michigan University, kindly shared data from his downburst wind field simulation, and Michael Kasperski, Ruhr-Universität Bochum, provided the Gaussian distribution of the modulus of rupture. Frank Holzäpfel commented on a draft of this paper. Our three anonymous referees provided insightful and inspiring comments. This work was partly funded by the German Ministry for Education and Research BMBF under contract 01LS05125 in the project RegioExAKT (*Regionales Risiko konvektiver Extremwetter-ereignisse: Anwenderorientierte Konzepte zur Trendbewertung und -anpassung*, Regional risk of convective extreme weather events: User-oriented concepts for trend assessment and adaptation).

References

Aran, M., J. Amaro, J. Arús, J. Bech, F. Figuerola, M. Gayà, and E. Vilaclara, 2009: Synoptic and mesoscale diagnosis of a tornado event in Castellcir, Catalonia, on 18th October 2006. *Atmos. Res.*, **93**(1-3), 147-160.

Baldwin, V. C., 1987: Green and dry-weight equations for above-ground components of planted Loblolly pines in the West Gulf region. *South. J. Appl. For.*, **11**, 212-218.

Bech, J., M. Gayà, M. Aran, F. Figuerola, J. Amaro, and J. Arús, 2007: Tornado damage analysis of a forest area using site survey observations, radar data and a simple analytical vortex model. Preprints, *4th European Conference on Severe Storms*, Trieste, 10-14 September 2007, 2 pp. [Available at www.essl.org/ECSS/2007/abs/02-Case-study/-1177974332.bech-1-sec02.oral.pdf]

Bech, J, M. Gayà, M. Aran, F. Figuerola, J. Amaro, and J. Arús, 2009: Tornado damage analysis of a forest area using site survey observations, radar data and a simple vortex model. *Atmos. Res.*, **93**(1-3), 118-130.

Beck, V., 2008: *Near-surface tornado wind field reconstruction from forest damage*. Diploma thesis, TU München, Munich, 162 pp. [Available at: www.essl.org/pdf/Beck2008.pdf]

Beck, V., and N. Dotzek, 2009: Reconstruction of near-surface tornado wind fields from forest damage. Preprints, *5th European Conf. on Severe Storms*, Landshut, 12-16 October 2009, 2 pp. [Available from www.essl.org/ECSS/2009/preprints/O11-05-beck.pdf]

Beck, V., N. Dotzek, R. Sausen, 2008: Determination of tornado intensity from forest damage. Preprints, *24th Conf. on Severe Local Storms*, Savannah, 27-31 October 2008, Amer. Meteor. Soc., Boston, 8 pp. [Available at ams.confex.com/ams/24SLS/-techprogram/paper_141809.htm]

Bluestein, H. B., 2007: Mobile Doppler radar observations of tornadoes. Preprints, *4th European Conf. on Severe Storms*, Trieste, 10-14 September 2007, 2 pp. [Available at www.essl.org/ECSS/2007/abs/05-Radars/bluestein-1177432754.pdf]

Blumenfeld, K. A., 2008: Comments on “Low-level winds in tornadoes and potential catastrophic tornado impacts in urban areas”. *Bull. Amer. Meteor. Soc.*, **89**(10), 1578-1579.

Brooks, H. E., 2004: On the relationship of tornado path length and width to intensity. *Wea. Forecasting*, **19**, 310-319.

Brooks, H. E., and C. A. Doswell III, 2001: Some aspects of the international climatology of tornadoes by damage classification. *Atmos. Res.*, **56**, 191-201.

Brooks, H. E., C. A. Doswell III, and D. Sutter, 2008: Comments on “Low-level winds in tornadoes and potential catastrophic tornado impacts in urban areas”. *Bull. Amer. Meteor. Soc*., **89**(1), 87-90.

Budney, L. J., 1965: Unique damage patterns caused by a tornado in dense woodlands. *Weatherwise*, **18**, 74-77, 86.

Davies-Jones, R. P., 1986: Tornado dynamics, 197-236. In: Kessler, E. (Ed.), *Thunderstorm Morphology and Dynamics*, 2nd ed. University of Oklahoma Press, Norman, 411 pp.

Doswell, C. A. III (Ed.), 2001: *Severe Convective Storms*. Meteor. Monogr., 28, Amer. Meteor. Soc., Boston, 561 pp.

Doswell, C. A. III, and D. W. Burgess, 1988: On some issues of United States tornado climatology. *Mon. Wea. Rev.*, **116**, 495-501.

Doswell, C. A. III, H. E. Brooks, and N. Dotzek, 2009: On the implementation of the Enhanced Fujita scale in the USA. *Atmos. Res.*, **93**(1-3), 554-563.

Dotzek, N., 2007: Derivation of physically motivated wind speed scales. Preprints, *4th European Conf. on Severe Storms*, Trieste, 10-14 September 2007, 2 pp. [Available at www.essl.org/ECSS/2007/abs/01-Theory/dotzek-2-sec01.oral-new.pdf]

Dotzek, N., 2009: Derivation of physically motivated wind speed scales. *Atmos. Res.*, **93**(1-3), 564-574.

Dotzek, N., and K. Friedrich, 2009: Downburst-producing thunderstorms in southern Germany: Radar analysis and predictability. *Atmos. Res.*, **93**(1-3), 457-473.

Dotzek, N., G. Berz, E. Rauch, and R. E. Peterson, 2000: Die Bedeutung von Johannes P. Letzmanns “Richtlinien zur Erforschung von Tromben, Tornados, Wasserhosen und Kleintromben” für die heutige Tornadoforschung. (The relevance of Johannes P. Letzmann's “Guidelines for research on tornadoes, waterspouts, and whirlwinds” for contemporary tornado research). *Meteorol. Z.*, **9**, 165-174. [In German, with English abstract, available at www.essl.org/people/dotzek/]

Dotzek, N., J. Grieser, and H. E. Brooks, 2003: Statistical modeling of tornado intensity distributions. *Atmos. Res.*, **67-68**, 163-187.

Dotzek, N., M. V. Kurgansky, J. Grieser, B. Feuerstein, and P. Névir, 2005: Observational evidence for exponential tornado intensity distributions over specific kinetic energy. *Geophys. Res. Lett*., **32**, L24813, doi:10.1029/2005GL024583.

Dotzek, N., P. Lang, M. Hagen, T. Fehr, and W. Hellmiss, 2007: Doppler radar observation, CG lightning activity, and aerial survey of a multiple downburst in southern Germany on 23 March 2001. *Atmos Res*., **83**, 519-533.

Dotzek, N., R. E. Peterson, B. Feuerstein, and M. Hubrig, 2008: Comments on "A simple model for simulating tornado damage in forests". *J. Appl. Meteor. Climatol*., **47**, 726-731.

Dotzek, N., P. Groenemeijer, B. Feuerstein, and A. M. Holzer, 2009: Overview of ESSL's severe convective storms research using the European Severe Weather Database ESWD. *Atmos. Res*., **93**(1-3), 575-586.

Euteneuer, G. A., 1970. Aerodynamische Betrachtungen im Pforzheimer Wirbelsturm vom 10. Juli 1968 (Aerodynamic considerations for the Pforzheim tornado of 10 July 1968). *Arch. Meteorol., Geophys. Bioklimatol*. A**19**, 355–371. [In German]

Forbes, G. S., and R. M. Wakimoto, 1983: A concentrated outbreak of tornadoes, downbursts and microbursts, and implications regarding vortex classification. *Mon. Wea. Rev.*, **111**, 220-235.

French, M. M, H. B. Bluestein, D. C. Dowell, L. J. Wicker, M. R. Kramar, and A. L. Pazmany, 2008: High-resolution, mobile Doppler radar observations of cyclic mesocyclogenesis in a supercell. *Mon. Wea. Rev*., **136**, 4997-5016.

Fujita, T. T., 1981: Tornadoes and downbursts in the context of generalized planetary scales. *J. Atmos. Sci.*, **38**, 1511-1534.

Fujita, T. T., 1989: The Teton-Yellowstone tornado of 21 July 1987. *Mon. Wea. Rev*., **117**, 1913-1940.

Gardiner, B. A., G. R. Stacey, R. E. Belcher, and C. J. Wood, 1997: Field and wind tunnel assessments of the implication of respacing and thinning for tree stability. *Forestry*, **70**, 233-252

Gardiner, B., S. Hale, A. Wellpott, and B. Nicoll, 2009: The development of a wind risk model for irregular stands. In: H. Mayer and D. Schindler (Eds.), Proc., *2nd International Conf. Wind Effects on Trees*, Freiburg, 13-16 October 2009, 127-133. Berichte des Meteorologischen Instituts der Albert-Ludwigs-Universität Freiburg, **19**, 340 pp. [Available at: www.wind2009.uni-freiburg.de/Abstractband_komplett_7.10.2009.pdf]

Hall, F., and R. D. Brewer, 1959: A sequence of tornado damage patterns. *Mon Wea. Rev*., **87**(6), 207-216.

Holland, A. P., A. J. Riordan, and E. C. Franklin, 2006: A simple model for simulating tornado damage in forests. *J. Appl. Meteor. Climatol*., **45**, 1597-1611.

Hubrig, M., 2004. Analyse von Tornado- und Downburst-Windschäden an Bäumen (Analysis of tornado and downburst wind damage to trees). *Forst und Holz*, **59**, 78-84. [In German, with English abstract, available under "References" at www.essl.org].

Kanak, K. M., 2005: Numerical simulation of dust devil-scale vortices. *Quart. J. Roy. Meteorol. Soc.*, **131**, 1271-1292.

Knupp, K. R., 2000: Narrow streaks of “straight-line” wind damage: Do tornadoes or microbursts produce them? Preprints, *20th Conf. on Severe Local Storms*, Orlando, 11-15 September 2000, Amer. Meteor. Soc., Boston, 644-645.

Lee, W.-C., and J. Wurman, 2005: Diagnosed three-dimensional axisymmetric structure of the Mulhall tornado on 3 May 1999. *J. Atmos. Sci.*, **62**, 2373-2393.

Letzmann, J. P., 1923: *Das Bewegungsfeld im Fuß einer fortschreitenden Wind- oder Wasserhose (The flow field at the base of an advancing tornado)*. Ph.D. Thesis, University Helsingfors. Acta et Commentationes Universitatis Dorpatensis **AVI.3**, C. Mattiesen Verlag, Dorpat, 136 pp. [In German, available at essl.org/pdf/Letzmann1923/-Letzmann1923.pdf]

Letzmann, J. P., 1925: Fortschreitende Luftwirbel (Advancing air vortices). *Meteorol. Z.*, **42**, 41-52. [In German]

Letzmann, J. P., 1939: *Richtlinien zur Erforschung von Tromben, Tornados, Wasserhosen und Kleintromben (Guidelines for research on tornadoes, waterspouts, and whirlwinds)*. Anlage XI, 91-110. In: Secretariat de l'Organisation Météorologique Internationale (Ed.), Klimatologische Kommission, Protokolle der Tagung in Salzburg, 13.-17. September 1937. IMO Publ. Nr. **38**, Edouard Ijdo, Leyde, 149 pp. [In German, available at essl.org/-pdf/Letzmann1939/Letzmann1939.pdf]

Lewellen, D. C., and W. S. Lewellen, 2007: Near-surface intensification of tornado vortices. *J. Atmos. Sci.*, **64**, 2176–2194.

Lewellen, D. C., B. Gong, and W. S. Lewellen, 2008: Effects of finescale debris on near-surface tornado dynamics. *J. Atmos. Sci.*, **65**, 3247–3262.

Müldner, W., 1950: Die Windbruchschäden des 22.7.1948 im Reichswald bei Nürnberg, ein Beispiel für ein Wirbelfeld als Teilerscheinung einer Böenfront (The wind damage of 22 July 1948 in the Reichswald forest near Nuremberg, an example of a vortex field as a local phenomenon of a gust front). *Berichte des Deutschen Wetterdienstes in der US-Zone*, **19**, 3-29. [In German]

Peltola, H., and S. Kellomäki, 1993: A mechanistic model for calculating windthrow and stem breakage of Scots pines at stand edge. *Silva Fenn.*, **27**, 99-111.

Peltola, H., S. Dupont, V.-P. Ikonen, H. Väisänen, A. Venälainen, and S. Kellomäki, 2009: The development of a wind risk model for irregular stands. In: H. Mayer and D. Schindler (Eds.), Proc., *2nd International Conf. Wind Effects on Trees*, Freiburg, 13-16 October 2009, 189-194. Berichte des Meteorologischen Instituts der Albert-Ludwigs-Universität Freiburg, **19**, 340 pp. [Available at: www.wind2009.uni-freiburg.de/-Abstractband_komplett_7.10.2009.pdf]

Peterson, C. J., 2003: Factors influencing treefall risk in tornadoes in natural forests. *Preprints, 83rd AMS Annual Meeting: Symposium on the F-Scale and Severe-Weather Damage Assessment*, Long Beach, Amer. Meteor. Soc., Boston, CD-ROM, P 3.1., 5 pp. [Available at ams.confex.com/ams/annual2003/techprogram/paper_53292.htm]

Peterson R. E., 1992a: Johannes Letzmann: A pioneer in the study of tornadoes. *Wea. Forecasting*, **7**(1), 166-184.

Peterson R. E., 1992b: Letzmann's and Koschmieder's "Guidelines for research on Funnels, tornadoes, waterspouts and whirlwinds". *Bull. Amer. Meteor. Soc.*, **73**(5), 597-611.

Potter, S., 2007: Fine-tuning Fujita. *Weatherwise*, **60**(2), 64-71.

Prandtl, L., 1925: Berichte über Untersuchungen zur ausgebildeten Turbulenz (Reports on investigations on fully developed turbulence). *Z. f. Angew. Math. u. Mech.*, **5**, 136-139. [In German]

Rossmann, F., 1959: Über Baumzerstörung durch Tromben, besonders durch Verdrehen der Bäume (On tree destruction by tornadoes, especially by torsion of the trees). *Meteor. Rdsch.*, **12**(5), 161-162. [In German]

Wegener, A., 1917: *Wind- und Wasserhosen in Europa (Tornadoes in Europe)*. Verlag Friedrich Vieweg und Sohn, Braunschweig, 301 pp. [In German, available under "References" at www.essl.org].

Wurman, J, 2002: The Multiple-Vortex Structure of a Tornado. *Wea. Forecasting*, **17**, 473-505.

Wurman, J., and C. R. Alexander, 2005: The 30 May 1998 Spencer, South Dakota, storm. Part II: Comparison of observed damage and radar-derived winds in the tornadoes. *Mon. Wea. Rev.*, **133**, 97-119.

Wurman, J., C. Alexander, P. Robinson, and Y. Richardson, 2007: Low-level winds in tornadoes and potential catastrophic tornado impacts in urban areas. *Bull. Amer. Meteor. Soc.*, **88**(1), 31-46.

Wurman, J., C. Alexander, P. Robinson, and Y. Richardson, 2008a: Reply. *Bull. Amer. Meteor. Soc.*, **89**(1), 90-94.

Wurman, J., C. Alexander, P. Robinson, and Y. Richardson, 2008b: Reply. *Bull. Amer. Meteor. Soc.*, **89**(10), 1580-1581.

Tables

Table 1: Homogenised wind speeds and increments of the Fujita- and TORRO-scales following Dotzek et al. (2000, 2003). For comparison, the corresponding steps on the Beaufort scale are given, also extending beyond the usual upper limits of B12 or B18.

	Sub-critical				Weak			
Fujita	F-2		F-1		F0		F1	
TORRO	T-4	T-3	T-2	T-1	T0	T1	T2	T3
Beaufort	B0, B1	B2, B3	B4, B5	B6, B7	B8, B9	B10, B11	B12, B13	B14, B15
v in m s^{-1}	0 - 3	3 - 7	7 - 12	12 - 18	18 - 25	25 - 33	33 - 42	42 - 51
v in km h^{-1}	0 - 11	11 - 25	25 - 43	43 - 65	65 - 90	90 - 119	119 - 151	151 - 184
	Significant							
	Strong				Violent			
Fujita	F2		F3		F4		F5	
TORRO	T4	T5	T6	T7	T8	T9	T10	T11
Beaufort	B16, B17	B18, B19	B20, B21	B22, B23	B24, B25	B26, B27	B28, B29	B30, B31
v in m s^{-1}	51 - 61	61 - 71	71 - 82	82 - 93	93 - 105	105 - 117	117 - 130	130 - 143
v in km h^{-1}	184 - 220	220 - 256	256 - 295	295 - 335	335 - 378	378 - 421	421 - 468	468 - 515

Table 2: Vortex parameters and velocity components derived from the damage analysis for the individual vortices of the Milosovice tornado. For the majority of these, a standard Rankine vortex was applied (cf. Beck, 2008).

Region	G_{max}	α in °	R_{max} in m	v_{trans} in m s^{-1}	v_{cir} in m s^{-1}	v_{max} in m s^{-1}
Ia	5.0	-140	80	16.5 ± 1.0	82.5 ± 5.0	99.0 ± 6.0
Ib	4.0	-140	80	16.5 ± 1.0	55.5 ± 4.0	82.5 ± 5.0
Ic	4.0	-150	80	16.5 ± 1.0	55.5 ± 4.0	82.5 ± 5.0
IIa	1.5	160	80	9.8 – 17.8	14.8 – 26.7	24.7 – 44.5
IIb	1.5	180	80	9.8 – 17.8	14.8 – 26.7	24.7 – 44.5
IIc	1.0	180	80	12.3 – 22.3	12.3 – 22.3	24.7 – 44.5
IIIa	1.0	0	40	12.4 – 22.3	12.4 – 22.3	24.7 – 44.5
IIIb	2.5	-90	40	7.1 – 12.7	17.6 – 31.8	24.7 – 44.5
IIIc	4.0	-90	60	4.9 – 8.9	19.8 – 35.6	24.7 – 44.5
IVa	4.0	150	60	4.9 – 8.9	19.8 – 35.6	24.7 – 44.5
IVb	4.0	120	60	4.9 – 8.9	19.8 – 35.6	24.7 – 44.5

Table 3: Velocity components and vortex parameters derived from the damage analysis of the Castellcir tornado. For all simulations, a standard Rankine vortex was applied (cf. Beck, 2008).

Region	G_{max}	α in °	R_{max} in m	v_{trans} in m s^{-1}	v_{cir} in m s^{-1}	v_{max} in m s^{-1}
I	2.0	0	50	11.0 ± 1.0	22.0 ± 2.0	33.0 ± 3.0
II	4.0	-90	50	11.0 ± 1.0	44.0 ± 4.0	55.0 ± 5.0
III	4.0	-90	50	11.0 ± 1.0	44.0 ± 4.0	55.0 ± 5.0
IV	3.5	-90	50	11.0 ± 1.0	38.5 ± 3.5	49.5 ± 4.5
V	3.5	-70	50	11.0 ± 1.0	38.5 ± 3.5	49.5 ± 4.5

Figure captions

Fig. 1: Velocity components used for the description of the tornado near-surface wind field. The circular velocity component v_{cir} is the vector sum of the radial (v_r) and tangential (v_θ) velocity components. The total velocity v at a point of the tornado wind field follows from the superposition of v_{cir} and the translation speed v_{trans}. Further, α denotes the angle between the wind direction (v) and v_r at the point of maximum velocity, φ is the angle between v_{cir} and v_{trans}, and finally, ψ is the angle between v and v_{trans}.

Fig. 2: Panels (a-c) show the vortex field for a constant angle $\alpha = 60°$ and varying values of $G_{max} = 0.75$ (a), $G_{max} = 1.0$ (b), and $G_{max} = 1.5$ (c). The separation into the two calm points occurs at $G_{max} = 1.0$. Panels (d-f) show the wind fields for a constant $G_{max} = 1.5$ and various angles $\alpha = -30°$ (d), $\alpha = -90°$ (e) and $\alpha = -120°$ (f). The resulting change from spiral inflow into the vortex centre (d) to spiral outflow of the vortex centre (f) becomes apparent. In each panel, tornado propagation is from bottom to top.

Fig. 3: (a) Analytically derived horizontal line cross-sections of tree damage patterns perpendicular to the track of the tornado (Letzmann, 1923) compared to (b) modelled horizontal line cross-sections of tree damage patterns for $G_{max} = 2.0$ and varying α and v_{crit}. For each angle α varying from α =0° to α =180°, tree damage patterns for different critical velocities for stem breakage (v_{crit}) are shown. For each angle α in both (a) and (b), v_{crit} increases from top to bottom. In (a), v_{crit} is indicated as multiples of the translation velocity v_{trans} (1.0, 1.5, 2.0, 2.5 times v_{trans}). In (b), the middle row of the damage patterns ($\alpha = -90°$) uses v_{crit} from the tree module for a spruce forest, while the upper and lower rows use minimum and maximum values ($v_{crit} - 25.0$ m s^{-1} and $v_{crit} + 25.0$ m s^{-1}), respectively. In each panel, tornado propagation is from bottom to top.

Fig. 4: Classification of the theoretical tree damage patterns into four different swath types (Letzmann, 1923) for $|\alpha| < 90°$, as a function of G_{max}. The damage patterns are shown for a counter clockwise rotation of the tornado vortex. For small values of $G_{max} < 1.0$, the tree with falling angle ψ=0° moves to the left for increasing values of the angle $|\alpha|$ and no crossing of trees occurs. The difference between swath type II and III is in the higher value of v_{crit} for swath type III that leads to a movement of the tree with ψ=0° to the right side of the damage pattern for increasing values of the angle $|\alpha|$. At $|\alpha| = 60°$ crossed trees can occur for both

swath types. High values of G_{max} are clearly indicated by a tree with ψ=180° (swath type IV). For $|\alpha| > 90°$, all tree damage patterns have a similar divergent structure. In each panel, tornado propagation is from bottom to top.

Fig. 5: Structure of the cross-section area A of tree against the wind consisting of two isosceles triangles for the crown and a rectangle for representing the stem. This is divided into 1-m segments Δz. The arrows indicate the directions of the acting forces (drag force F_W and gravitational force F_G) and $x(z)$ is the bend-over distance of the tree.

Fig. 6: Structure of the complete model consisting of a tree damage module for the calculation of v_{crit} and a wind field module calculating the instantaneous wind velocity at each grid point. If the instantaneous wind velocity exceeds v_{crit}, the tree is considered to be broken. The structure of the model allows introducing other tree damage or wind field modules in the future to calculate the specific model parameters.

Fig. 7: (a) Aerial photograph of the forest damage produced by the Milosovice tornado (courtesy of Martin Setvák, CHMI), showing the division of the damage patterns into one main vortex (red) and three smaller vortices. (b) Digitised damage patterns containing the trace (dashed line) as well as the divergence and convergence lines (dash-dotted line) of the individual vortices. In both panels, the blue arrow points north, and the black arrow indicates the propagation of the tornado towards the east-south-east.

Fig. 8: In each of the panels, simulated damage patterns (lower left) are compared to the observed damage patterns (top) of the main vortex of the Milosovice tornado. From the simulated damage patterns, which are more regular than the observed ones, the tornado near-surface wind fields are derived. On the right, the corresponding F-scale area distribution along the path is shown. Tornado propagation is from bottom to top.

Fig. 9: Reconstructed near-surface tornado wind fields from the Milosovice damage patterns for the main vortex (I) and the three smaller vortices (II), (III) and (IV) indicating spiral outflow for the vortices (I), (II) and (IV). The vortices (I) and (III) have cyclonic sense of rotation while the vortices (II) and (IV) were anticyclonic. For the simulation, a standard Rankine vortex was used.

Fig. 10: Analysis of the Castellcir tornado: On the left, the location of the broken trees is shown (after Bech et al., 2009) chronologically divided into regions (I)-(V). In the middle column, the simulated tree damage patterns are illustrated, as well as the boxes used for comparison to the observed damage pattern. The F-scale area distribution for each region is given in the right column. As the obtained parameters from region II and III are identical, only one simulation was performed. Tornado propagation is from bottom to top.

Fig. 11: Comparison of the simulated damage patterns of (a) Holland (2006) and (b) the present study for a fixed G_{max} = 3.5 and α = 80° (1), 73° (2), 63° (3) and 51° (4). From (1) to (4) the radial velocity component v_r increases while the tangential velocity component v_{tan} decreases and the translation velocity component v_{trans} is held constant. Panel (b) shows more broken trees compared to panel (a), while the structure of the tree damage patterns are very similar. The blue lines indicate the convergence lines identified by a tree with fall angle ψ = 0°, while the orange convergence line is identified by a tree with fall angle ψ = 180°. The characteristic convergent tree damage patterns for inflow into the vortex centre for angles of $|\alpha|$ < 90° are notable in both (a) and (b). A random distribution of tree age is used in both panels and the tornado propagation is from bottom to top.

Fig. 12: (1) Wind fields and (2) streamline patterns produced by our wind field module compared to (3) streamline patterns from Letzmann (1923) for a tornado with double wind speed maximum. Accordingly, α increases and decreases twice. The starting angle α in the vortex centre increases from α = -120° (a) to α = -90° (b) and α = -60° (c).

Figures

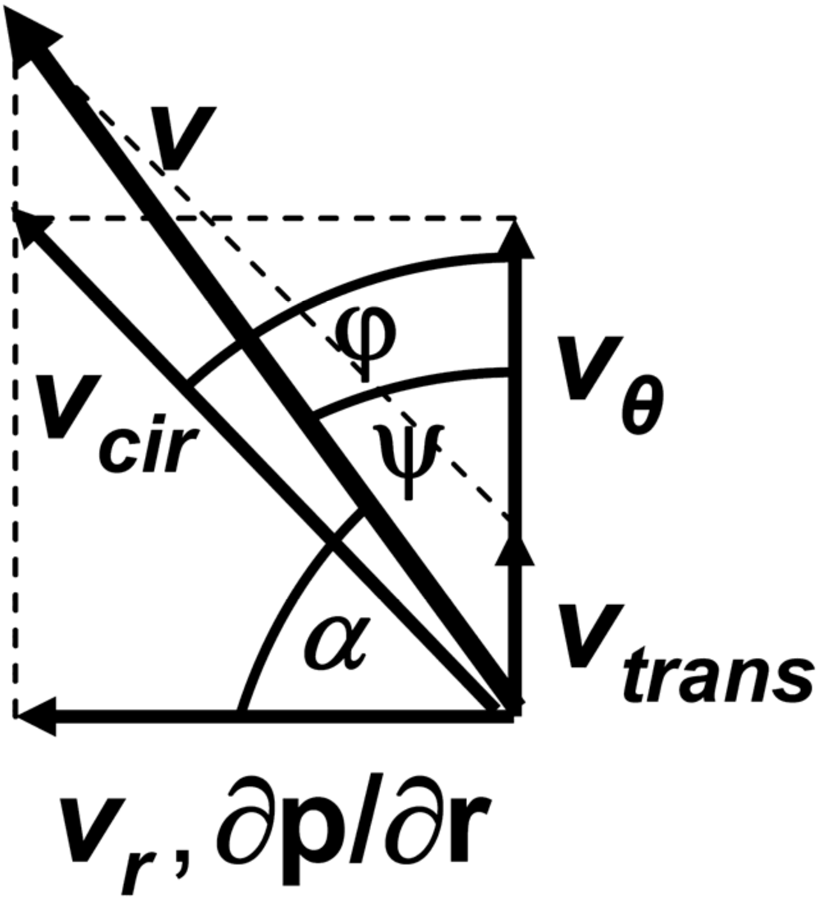

Fig. 1: Velocity components used for the description of the tornado near-surface wind field. The circular velocity component v_{cir} is the vector sum of the radial (v_r) and tangential (v_θ) velocity components. The total velocity v at a point of the tornado wind field follows from the superposition of v_{cir} and the translation speed v_{trans}. Further, α denotes the angle between the wind direction (v) and v_r at the point of maximum velocity, φ is the angle between v_{cir} and v_{trans}, and finally, ψ is the angle between v and v_{trans}.

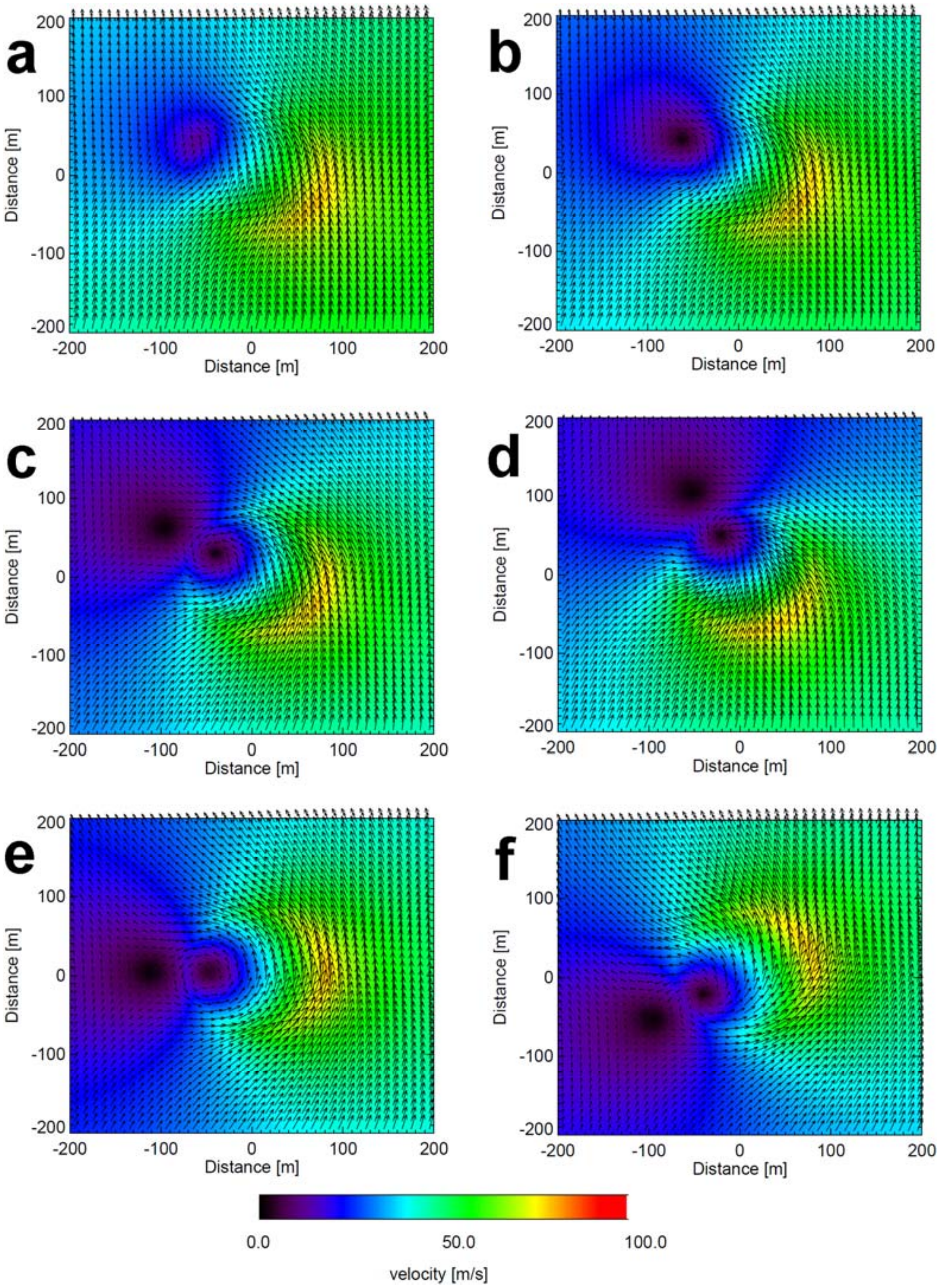

Fig. 2: Panels (a-c) show the vortex field for a constant angle α = 60° and varying values of G_{max} = 0.75 (a), G_{max} = 1.0 (b), and G_{max} = 1.5 (c). The separation into the two calm points occurs at G_{max} = 1.0. Panels (d-f) show the wind fields for a constant G_{max} = 1.5 and various angles α = -30° (d), α = -90° (e) and α = -120° (f). The resulting change from spiral inflow into the vortex centre (d) to spiral outflow of the vortex centre (f) becomes apparent. In each panel, tornado propagation is from bottom to top.

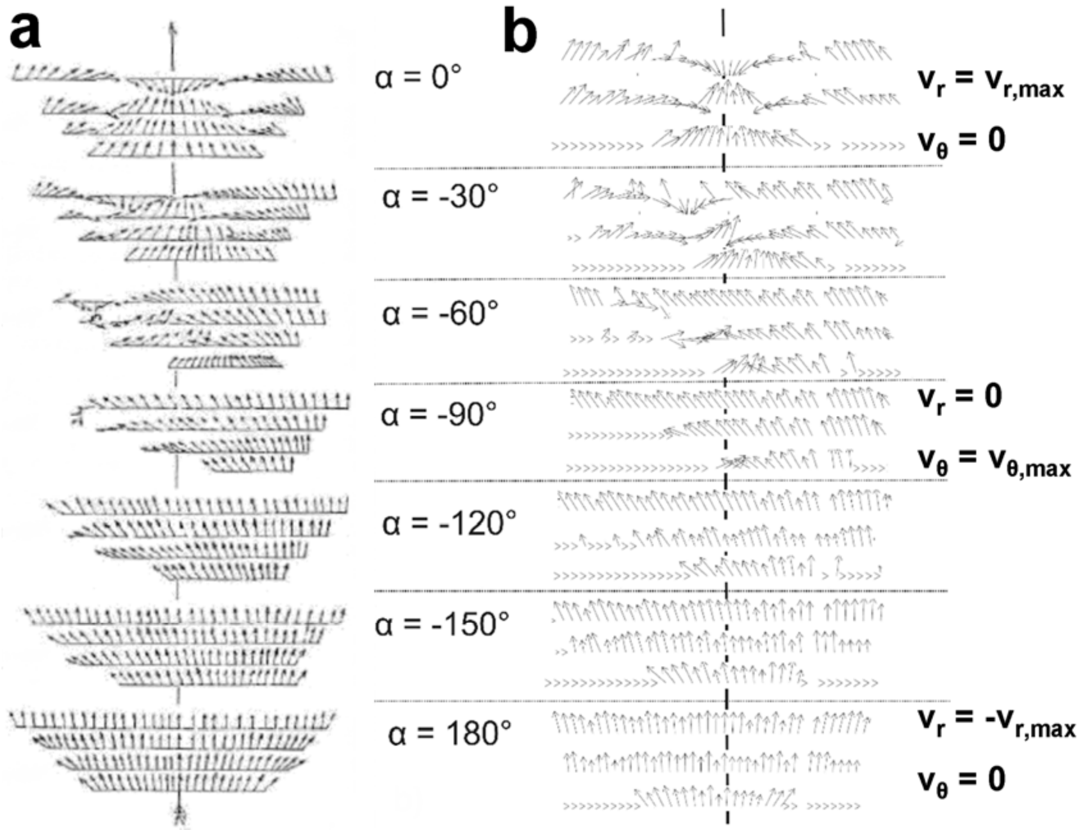

Fig. 3: (a) Analytically derived horizontal line cross-sections of tree damage patterns perpendicular to the track of the tornado (Letzmann, 1923) compared to (b) modelled horizontal line cross-sections of tree damage patterns for G_{max} = 2.0 and varying α and v_{crit}. For each angle α varying from α =0° to α =180°, tree damage patterns for different critical velocities for stem breakage (v_{crit}) are shown. For each angle α in both (a) and (b), v_{crit} increases from top to bottom. In (a), v_{crit} is indicated as multiples of the translation velocity v_{trans} (1.0, 1.5, 2.0, 2.5 times v_{trans}). In (b), the middle row of the damage patterns (α = -90°) uses v_{crit} from the tree module for a spruce forest, while the upper and lower rows use minimum and maximum values (v_{crit} – 25.0 m s^{-1} and v_{crit} +25.0 m s^{-1}), respectively. In each panel, tornado propagation is from bottom to top.

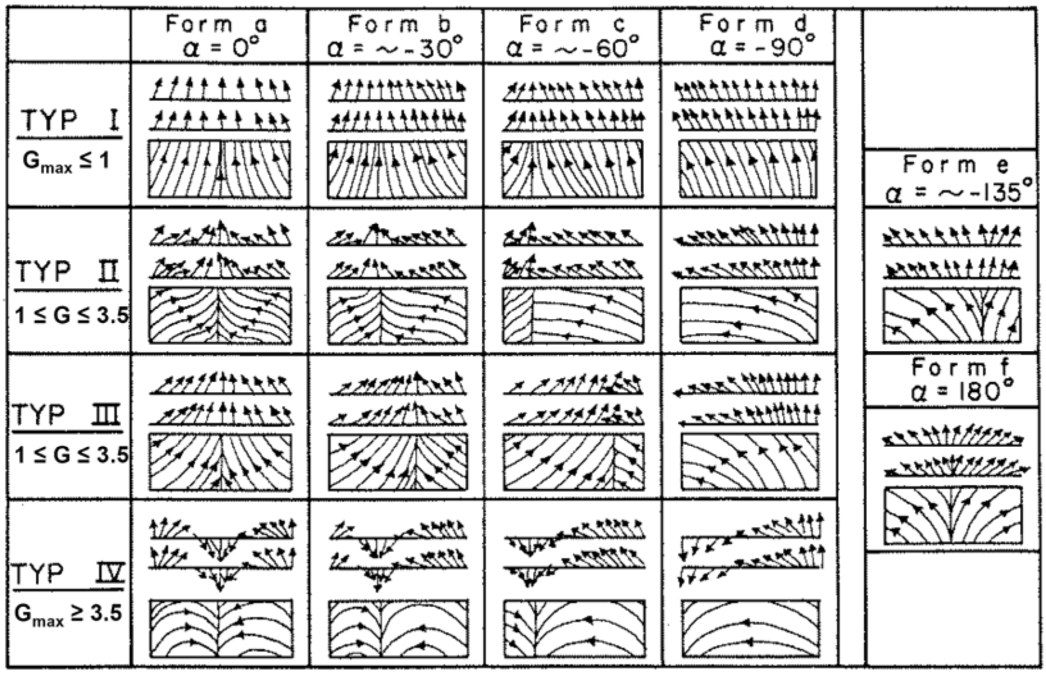

Fig. 4: Classification of the theoretical tree damage patterns into four different swath types (Letzmann, 1923) for $|\alpha| < 90°$, as a function of G_{max}. The damage patterns are shown for a counter clockwise rotation of the tornado vortex. For small values of $G_{max} < 1.0$, the tree with falling angle $\psi=0°$ moves to the left for increasing values of the angle $|\alpha|$ and no crossing of trees occurs. The difference between swath type II and III is in the higher value of v_{crit} for swath type III that leads to a movement of the tree with $\psi=0°$ to the right side of the damage pattern for increasing values of the angle $|\alpha|$. At $|\alpha| = 60°$ crossed trees can occur for both swath types. High values of G_{max} are clearly indicated by a tree with $\psi=180°$ (swath type IV). For $|\alpha| > 90°$, all tree damage patterns have a similar divergent structure. In each panel, tornado propagation is from bottom to top.

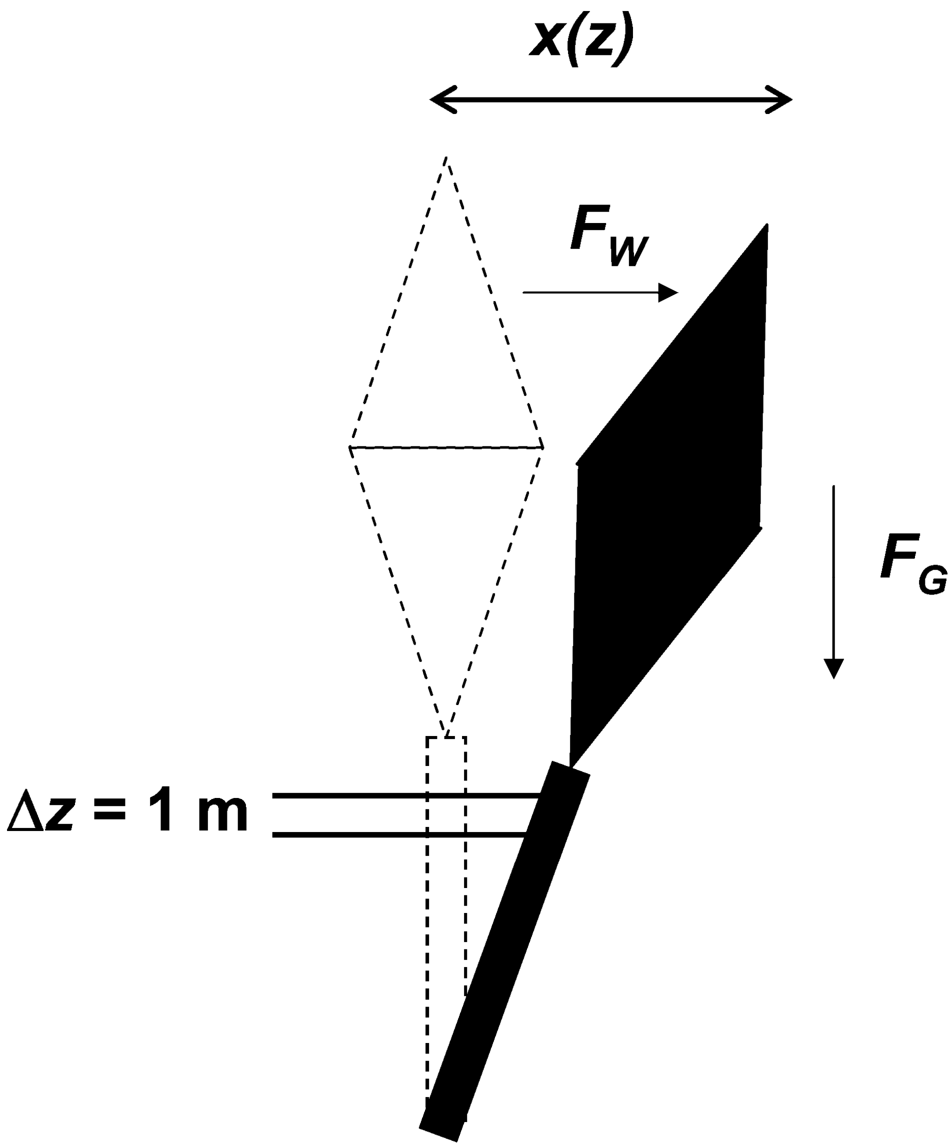

Fig. 5: Structure of the cross-section area A of tree against the wind consisting of two isosceles triangles for the crown and a rectangle for representing the stem. This is divided into 1-m segments Δz. The arrows indicate the directions of the acting forces (drag force F_W and gravitational force F_G) and $x(z)$ is the bend-over distance of the tree.

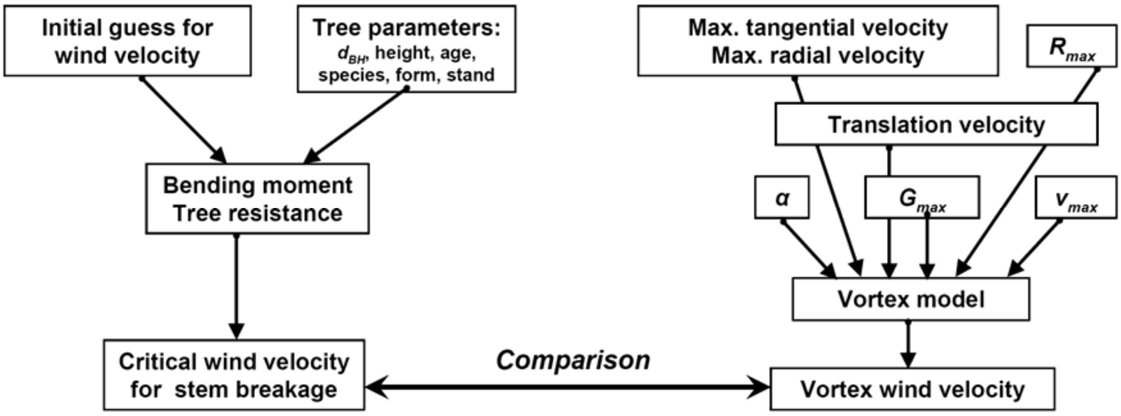

Fig. 6: Structure of the complete model consisting of a tree damage module for the calculation of v_{crit} and a wind field module calculating the instantaneous wind velocity at each grid point. If the instantaneous wind velocity exceeds v_{crit}, the tree is considered to be broken. The structure of the model allows introducing other tree damage or wind field modules in the future to calculate the specific model parameters.

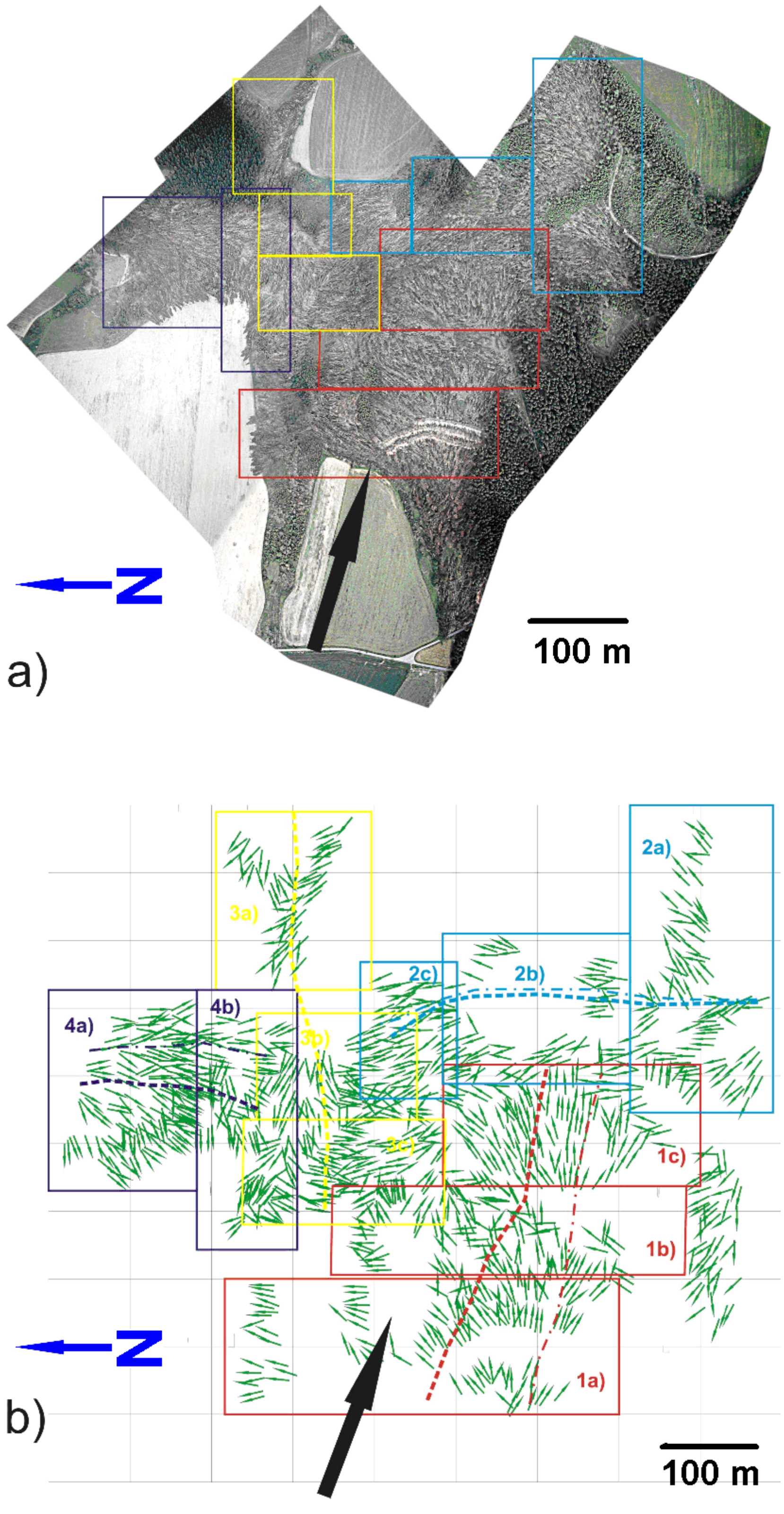

Fig. 7: (a) Aerial photograph of the forest damage produced by the Milosovice tornado (courtesy of Martin Setvák, CHMI), showing the division of the damage patterns into one main vortex (red) and three smaller vortices. (b) Digitised damage patterns containing the trace (dashed line) as well as the divergence and convergence lines (dash-dotted line) of the individual vortices. In both panels, the blue arrow points north, and the black arrow indicates the propagation of the tornado towards the east-south-east.

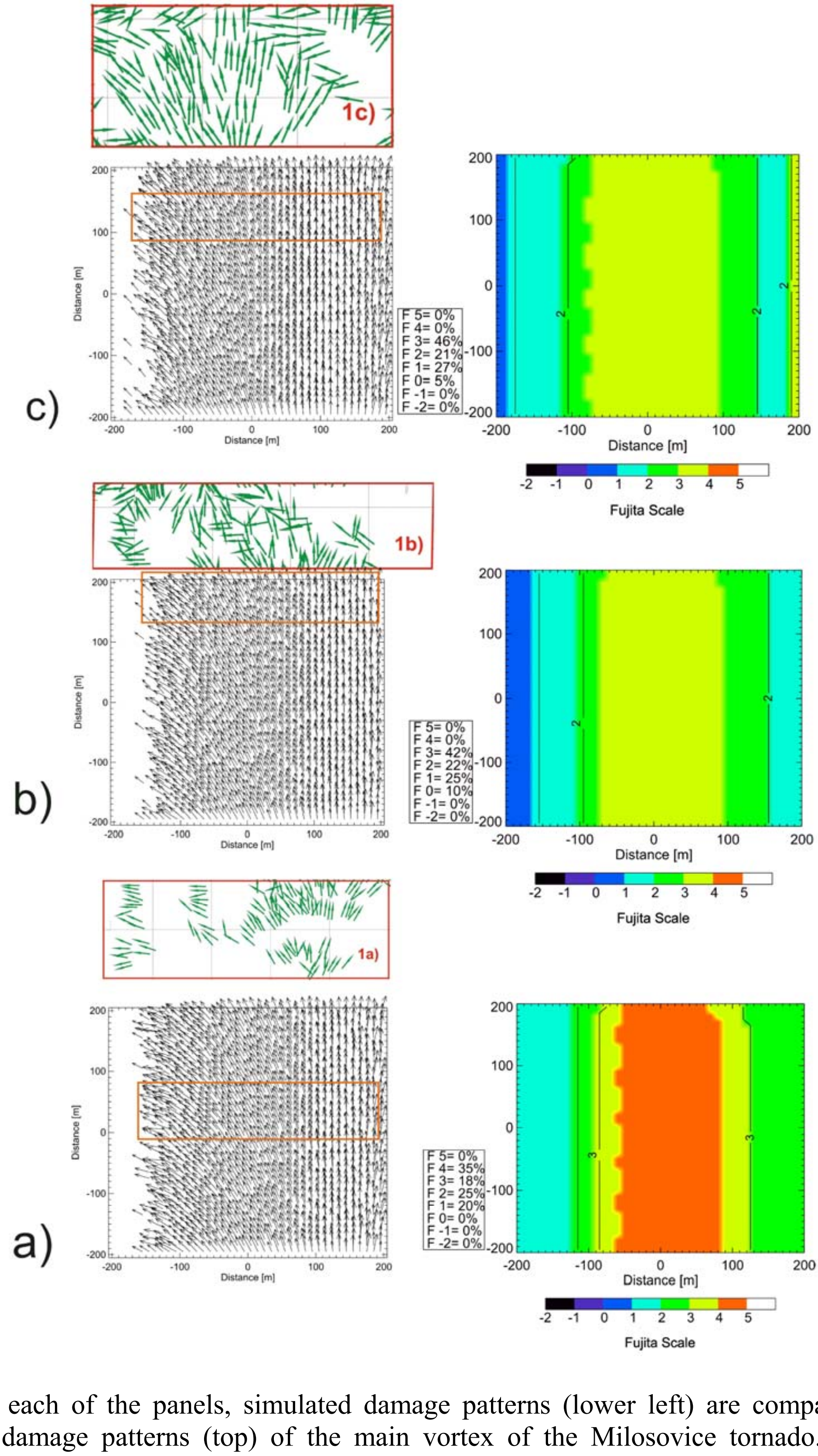

Fig. 8: In each of the panels, simulated damage patterns (lower left) are compared to the observed damage patterns (top) of the main vortex of the Milosovice tornado. From the simulated damage patterns, which are more regular than the observed ones, the tornado near-surface wind fields are derived. On the right, the corresponding F-scale area distribution along the path is shown. Tornado propagation is from bottom to top.

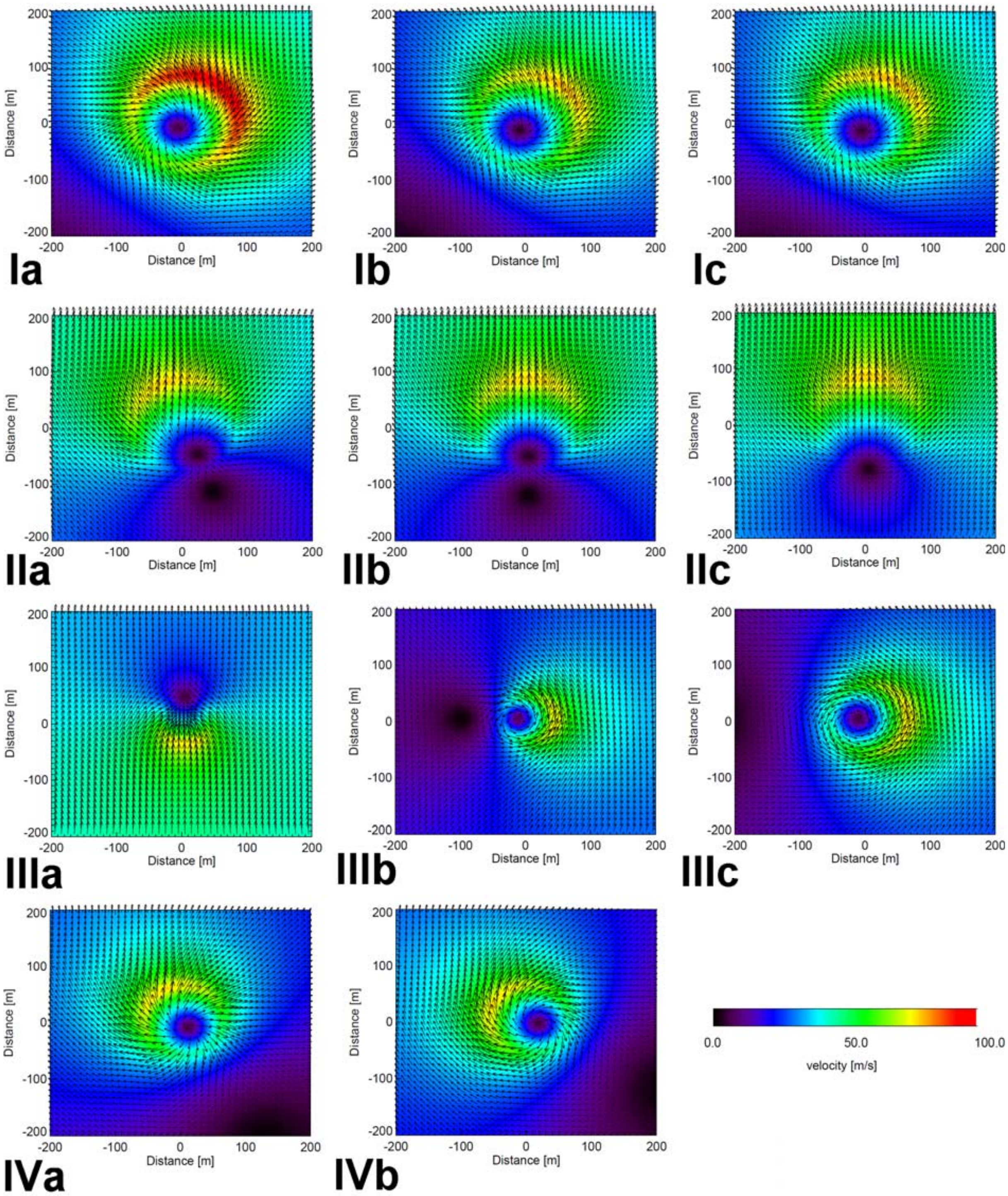

Fig. 9: Reconstructed near-surface tornado wind fields from the Milosovice damage patterns for the main vortex (I) and the three smaller vortices (II), (III) and (IV) indicating spiral outflow for the vortices (I), (II) and (IV). The vortices (I) and (III) have cyclonic sense of rotation while the vortices (II) and (IV) were anticyclonic. For the simulation, a standard Rankine vortex was used.

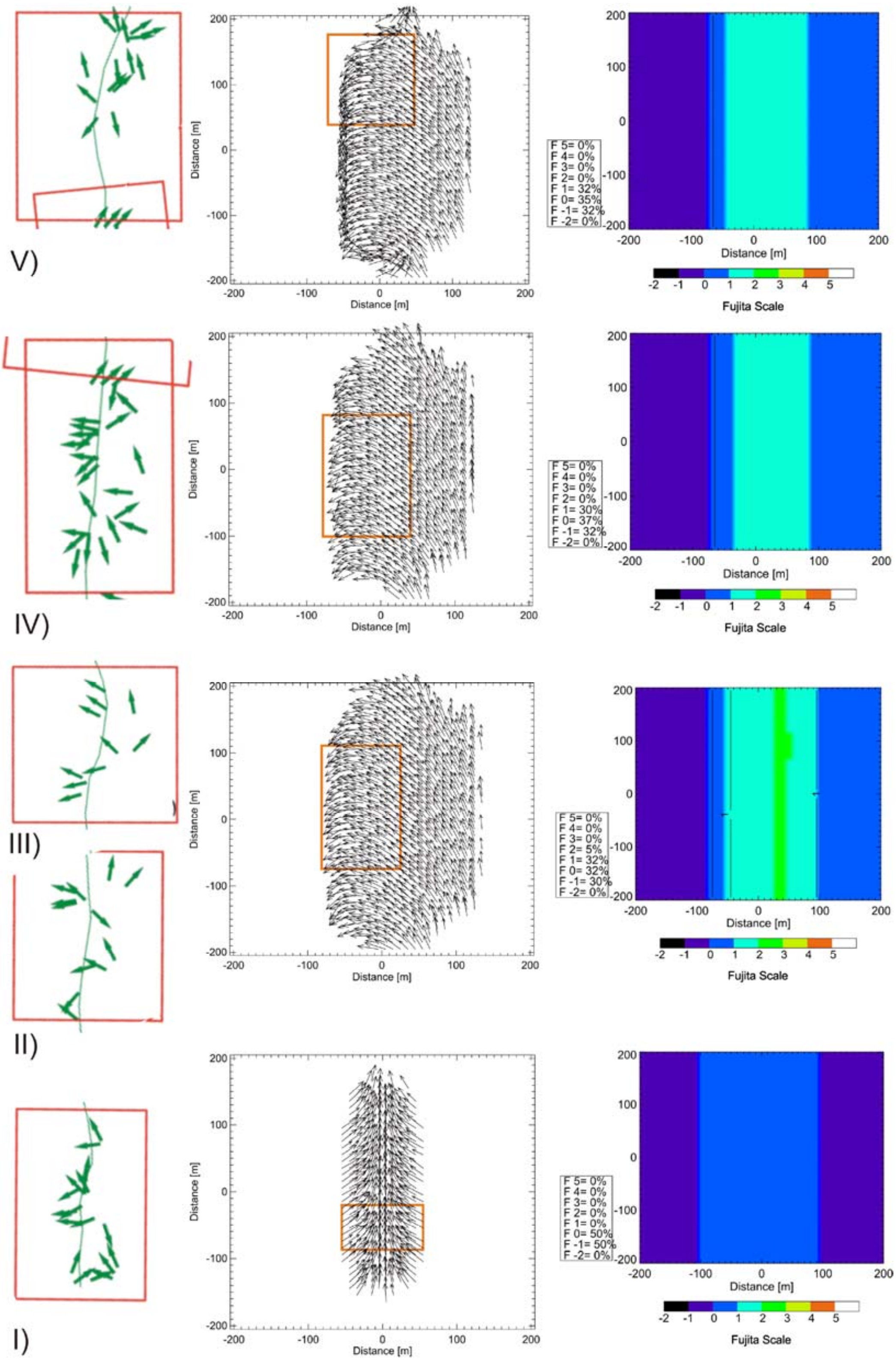

Fig. 10: Analysis of the Castellcir tornado: On the left, the location of the broken trees is shown (after Bech et al., 2009) chronologically divided into regions (I)-(V). In the middle column, the simulated tree damage patterns are illustrated, as well as the boxes used for comparison to the observed damage pattern. The F-scale area distribution for each region is given in the right column. As the obtained parameters from region II and III are identical, only one simulation was performed. Tornado propagation is from bottom to top.

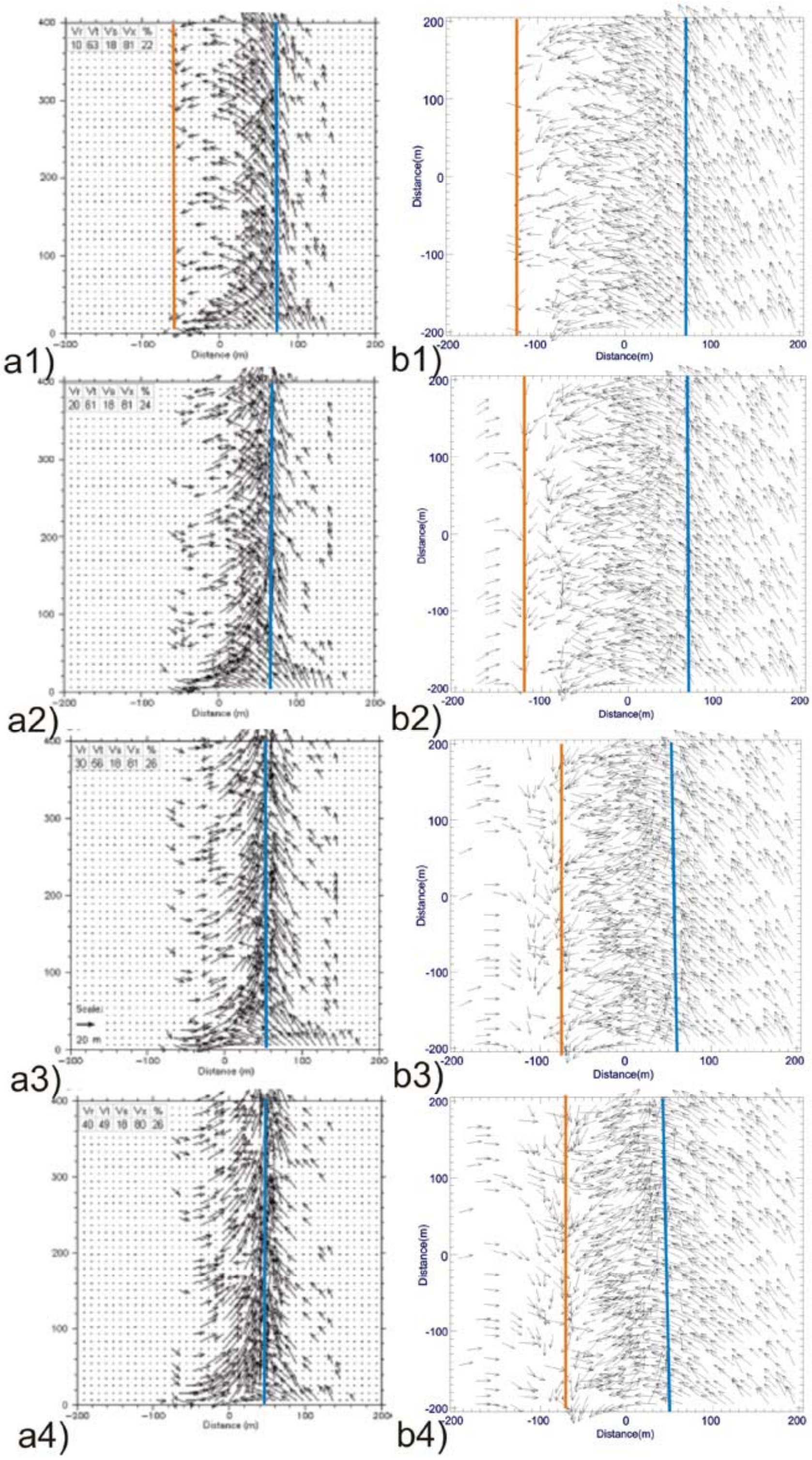

Fig. 11: Comparison of the simulated damage patterns of (a) Holland (2006) and (b) the present study for a fixed G_{max} = 3.5 and α = 80° (1), 73° (2), 63° (3) and 51° (4). From (1) to (4) the radial velocity component v_r increases while the tangential velocity component v_{tan} decreases and the translation velocity component v_{trans} is held constant. Panel (b) shows more broken trees compared to panel (a), while the structure of the tree damage patterns are very similar. The blue lines indicate the convergence lines identified by a tree with fall angle ψ = 0°, while the orange convergence line is identified by a tree with fall angle ψ = 180°. The characteristic convergent tree damage patterns for inflow into the vortex centre for angles of $|\alpha|$ < 90° are notable in both (a) and (b). A random distribution of tree age is used in both panels and the tornado propagation is from bottom to top.

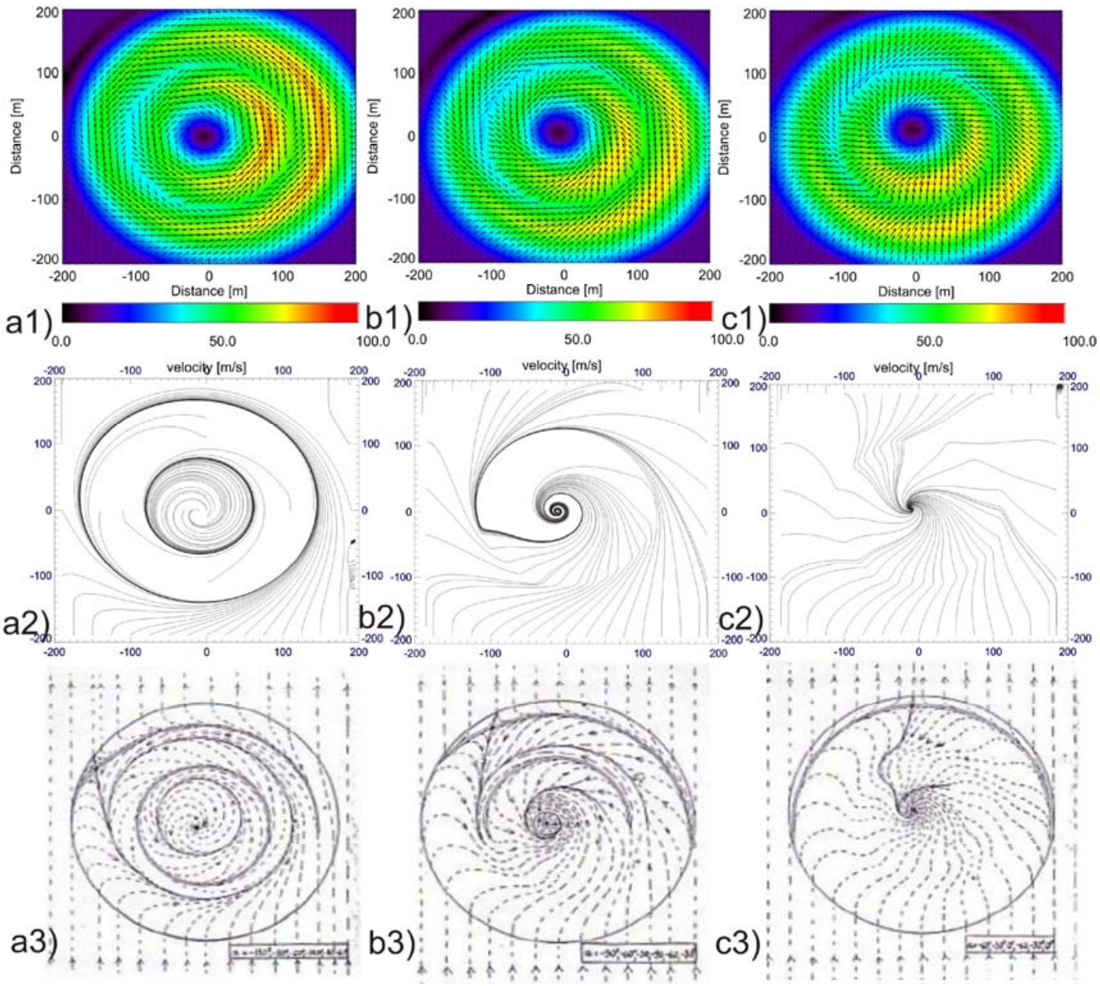

Fig. 12: (1) Wind fields and (2) streamline patterns produced by our wind field module compared to (3) streamline patterns from Letzmann (1923) for a tornado with double wind speed maximum. Accordingly, α increases and decreases twice. The starting angle α in the vortex centre increases from α = -120° (a) to α = -90° (b) and α = -60° (c).